MODIFICATION OF NANOHOOP FLUOROPHORES TO IMPROVE USE IN BIOLOGICAL IMAGING

by

ZACH GARRISON

A THESIS

Presented to the Department of Chemistry
and the Robert D. Clark Honors College
in partial fulfillment of the requirements for the degree of
Bachelor of Science

June 2020

An Abstract of the Thesis of

Zach Garrison for the degree of Bachelor of Science
in the Department of Chemistry to be taken June 2020

Title: Modification of Nanohoop Fluorophores to Improve Use in Biological Imaging

Approved: _____ *Ramesh Jasti, Ph.D.* _____
Primary Thesis Advisor

Biological imaging is an extremely important tool for biological and medical research. It allows researchers and doctors to access a perspective of biological systems not available with the naked eye. However, the quality of the images and the subsequent discoveries that come from those images depends on the quality of the reporter molecule (i.e fluorophore) used. As such, there is a wide variety of commercially available fluorophores that emit light all along the visible spectrum. Unfortunately, many of these commercially available fluorophores suffer from limitations that restrict their imaging applications. This would make the introduction of a new fluorophore that overcomes these limitations a valuable discovery.

One molecular structure that does not suffer from those same limitations is a cycloparaphenylene (CPP), which is a symmetrical arrangement of phenyl rings linked at the *para*-position. These nanohoop structures have unique size dependent fluorescent properties and can be controllably synthesized to possess characteristics desired for a variety of applications. This project was able to make further modifications to the nanohoop structure that unlocked new colors and worked towards improving the conjugation of the molecules to biological entities.

Acknowledgements

This project was funded by the National Science Foundation (NSF) grant number CHE-1800586, and the UO OHSU Seed Grant Program.

I would like to thank Professor Casey Shoop for his advice and friendship over the years and throughout this research process. My honors college experience has been profoundly enriched by our debates in class and our chats in his office.

I would like to thank Professor Ramesh Jasti for giving me the opportunity to be a member of his research group and allowing me to explore the topics and research areas that I am most interested in. Additional gratitude goes to my fellow members of the Jasti lab who have welcomed and encouraged me over the last two years. Their dedication has inspired my work ethic inside and out of the lab.

I would like to thank my graduate mentor Terri Lovell for all her help over the last two years. Her guidance and patience allowed me to learn more than I have in any classroom. Nothing that I have accomplished in the lab or on this thesis project would have been possible without her contributions. Terri's unwavering standards of excellence and her outstanding work ethic are an inspiration.

Lastly, I would like to thank my friends and family for their love and support over the years. Their encouragement has motivated me throughout my undergraduate and research journey.

Table of Contents

List of Figures

Chapter I. Background

I.I Fluorescence and Common Fluorophores

Fluorophores are extremely valuable tools used to visualize biological processes that normally remain hidden to the human eye. Absorbance is initiated when a photon of suitable energy excites an electron in ground state of the molecule. The electron raises in energy to an excited state, and then relaxes to the lowest excited state. Further decay from the excited state causes the emission of a photon of light (fluorescence). Figure 1[1]. depicts the full excitation and light releasing process.

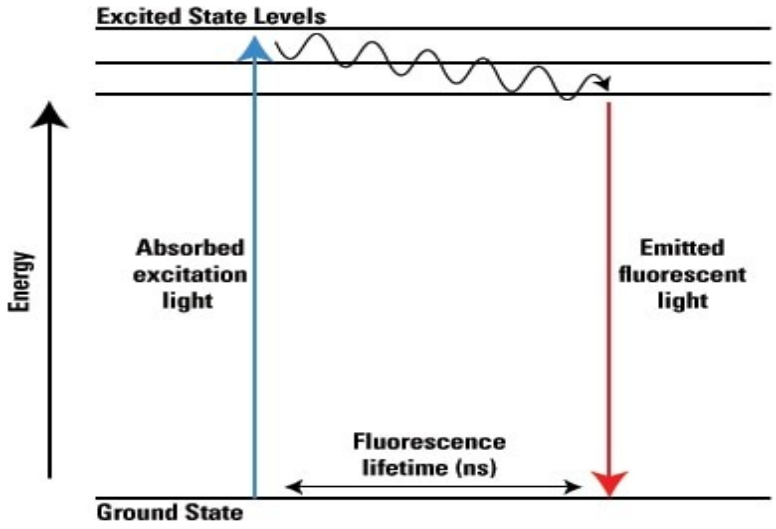

Figure 1. Fluorophore Excitation

The brightness of a fluorophore is characterized by its quantum yield and extinction coefficient. The quantum yield is a representation of how many photons of light are emitted relative to the number of photons used to excite the fluorophore, i.e. the fluorophores light emitting efficiency. The extinction coefficient is a measure of how well the molecule absorbs light. Together, the quantum yield and extinction coefficient represent how bright a molecule appears, therefore high values of either correlate to greater brightness[2].

Fluorophores have a wide range of applications in biological research and in the medical field. Some of these uses include structural identification and disease detection. For those applications, the fluorophore is attached to a biomolecule or targeting moiety which targets a specific structure the user desires to image. For example, if a researcher wanted to image a specific protein in a cell, they would attach a biomolecule that specifically binds to that protein. When the fluorophore is introduced into the cell, it will exclusively bind to the protein of interest and illuminating its structure. In the case of disease detection, a fluorophore is attached to a biomolecule that can identify the disease or antigen allowing for location and identification of the disease.

Fluorophores come in a variety of structures and colors. The emission of a fluorophore is dictated by the energy gap between the Highest Occupied Molecular Orbital (HOMO) and Lowest Unoccupied Molecular Orbital (LUMO). These orbitals are used as a way to describe where the electrons are in the molecule (its electronic structure). As the HOMO-LUMO gap shrinks, the emission of the fluorophore becomes more red in color (Figure 2). Conversely, as the HOMO-LUMO gap widens, the emission profile becomes more blue-shifted. The HOMO and LUMO of a molecule are a result of the structure of the molecule[3].

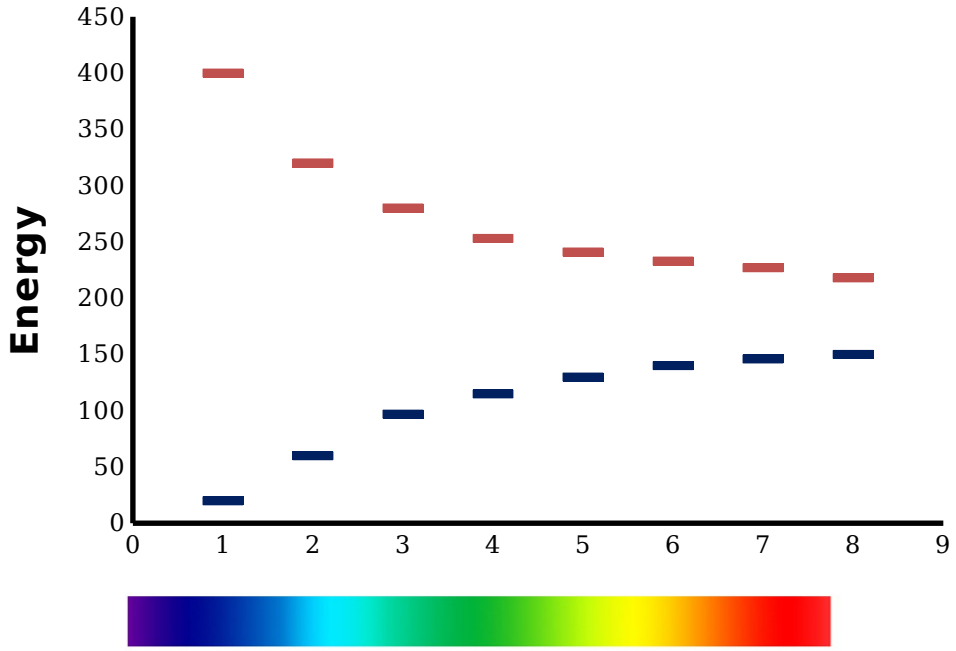

Figure 2. HOMO-LUMO Gap and Emission Profiles

Commercially available fluorophores are mainly based on four fluorescent scaffolds shown in Figure 3[3]. These fluorophores have been widely used in biological applications but suffer from some limitations. For example, a commonly used fluorophore, fluorescein (**1c**), is non-fluorescent at biological pH due to a structural change[4]. Another prevalent issue occurs with long or repeated exposure to an excitation light source, which causes the fluorophore structure to change to a non-fluorescent conformation. This process is called photobleaching and is common with flu (**1c**) and cyanine (**1a**)[5]. Coumarin dyes (**1d**) have inherently low brightness limiting the applications it can be used in[3]. Lastly, fluorophores with blue absorptions are to cells and blue emitting fluorophores suffer from low signal to noise producing low quality images. Therefore, fluorophores that absorb and emit in the red region are desirable but tend to have lower quantum yields resulting in low brightness[6]. These limitations create an incentive for the development of new fluorophore scaffolds that overcome these limitations.

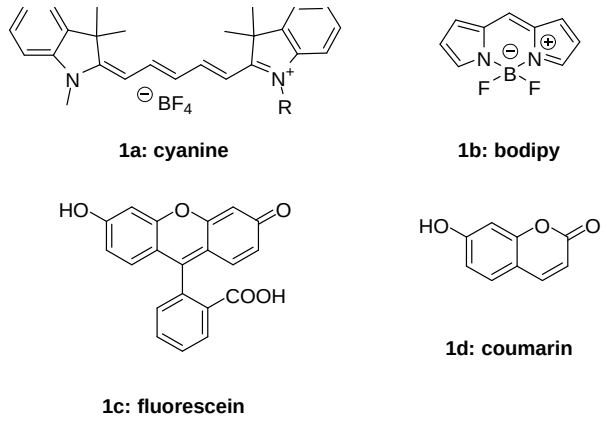

Figure 3. Four Main Fluorophore Scaffolds

I.II Cycloparaphenylenes as a Novel Fluorescent Scaffold

One exciting structure that may offer a solution to the fluorophore limitations outlined in the previous section are cycloparaphenylenes (CPPs), which are often called nanohoops (Figure 4). CPPs are macrocycles containing benzene rings linked in the *para*-position, which represent a small slice of a carbon nanotube (CNT) seen in Figure 4.

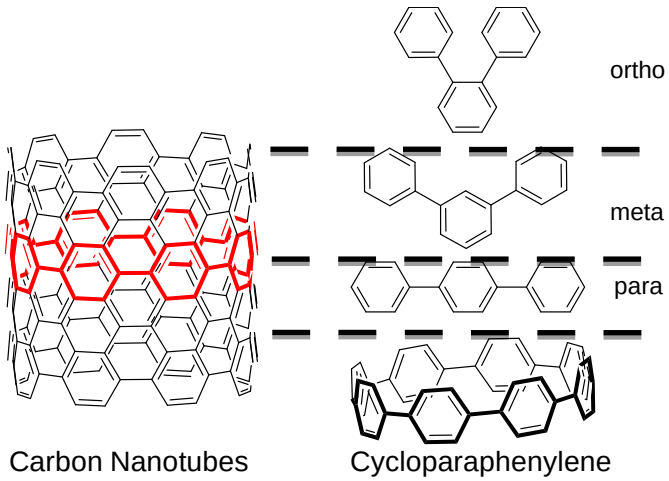

Figure 4. Carbon Nanotubes and Cycloparaphenylene

CNTs are carbon-based materials that are useful as strength reinforcing materials and components in electronic devices[7]. Unfortunately, the synthesis of CNTs is not easily controlled and results in a mixture of undesired sizes and lengths. Therefore, CPPs were

initially sought after as foundational building blocks to assemble CNTs[8]. CPPs are controllably synthesized via synthetic organic chemistry, therefore their structure is easily modified to include a variety of functional groups[9–11]. The synthesis of CPPs involves a series of reactions which add small building blocks together to form larger curved pieces used to make the final nanohoop structure.

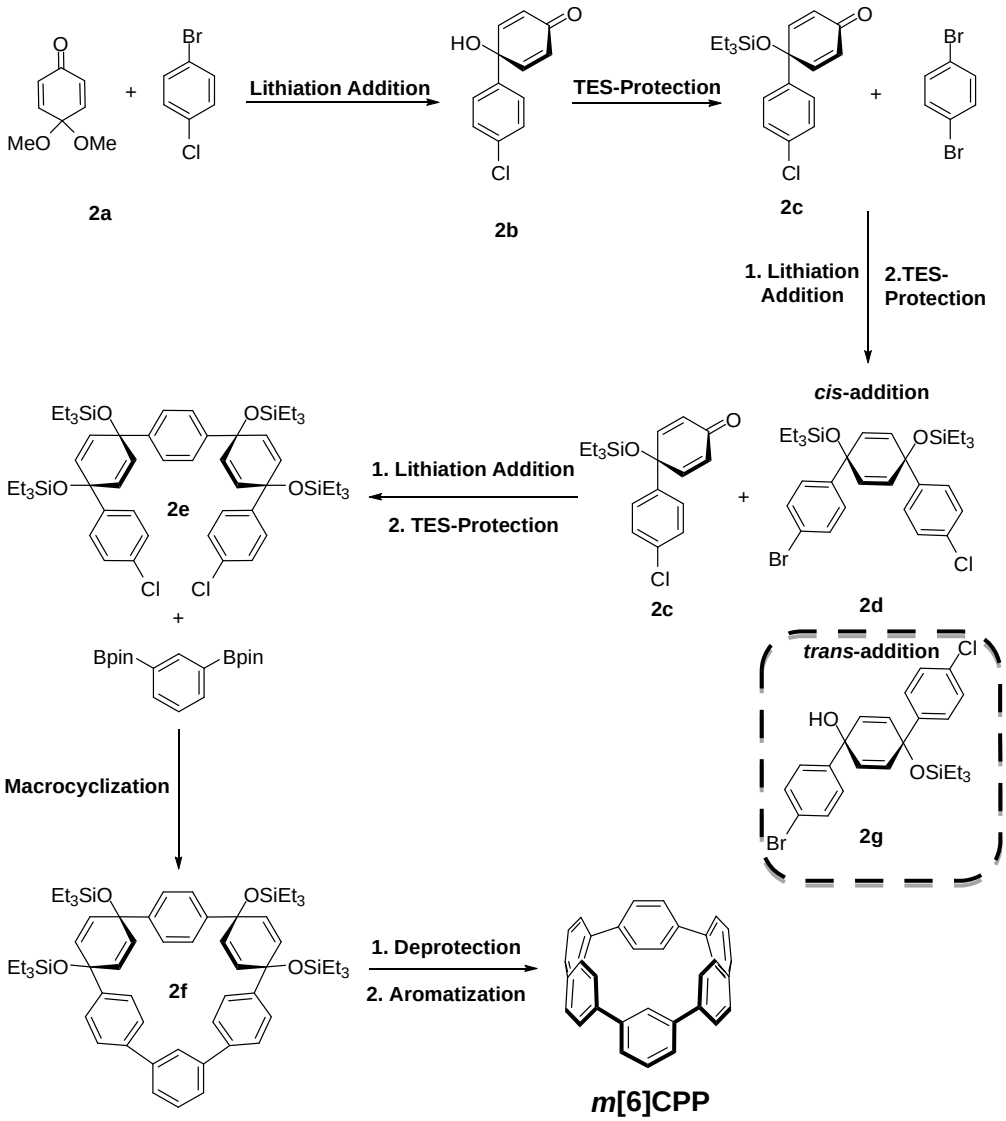

Figure 5. Synthetic Scheme of ***m*[6]CPP**

The initial steps involve lithiation additions (see methods and materials) to create new carbon-carbon bonds facilitated by lithium halogen exchange (**2a-b**). To force the

necessary curvature to form the nanohoop, large protecting groups (triethylsilyl or $SiEt_3$) are used to sterically facilitate a *cis*-addition (**2d**) as opposed to a *trans*-addition (**2g**)[12]. The series of lithiation additions and triethylsilyl (TES) protections are repeated to form the larger curved pieces (**2e**). The large curved piece is then used to form a cyclic structure via Suzuki cross coupling (**2e-f**). Once the macrocycle has been formed, the cyclohexadienes are converted to benzenes to give the completed macrocycle (***m*[6]CPP**)[13].

One of the most interesting features of CPPs are their photophysical properties. Contrary to standard photophysical trends with linear assemblies of benzene rings where the molecule tends to blueshift as the number of rings is reduced, the fluorescence trend of CPPs red-shifts as the number of rings is reduced (and the hoop size decreases)[14].This trend corresponds to a shrinking of the HOMO-LUMO gap as ring size decreases which is influenced by the circular nature of the CPP structure.

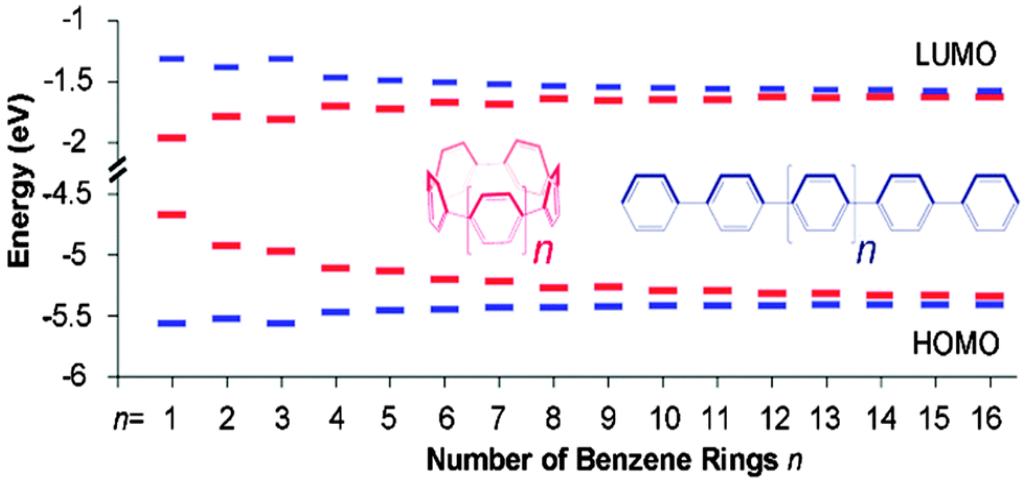

Figure 6. HOMO and LUMO energies of CPPs (blue) and Linear (red)[14]

CPPs also possess high extinction coefficients, and the larger sizes have high quantum yields making them bright molecules. For example, [12]CPP is over 40 times brighter than fluorescein[15]. These characteristics present an opportunity to harness the CPP

structure to design a new fluorophore scaffold that would not be susceptible to the same limitations as many commonly used fluorophores.

Due to the synthetic control, the photophysical properties of CPPs can be enhanced by making simple structural adjustments to the structure. One adjustment allowed fluorescence in previously non-fluorescent nanohoops as well as a large increase in brightness of other sizes. This key adjustment involved altering the position of a single bond within the nanohoop from a *para*- linkage to a *meta*- linkage as shown in Figure 7[13].

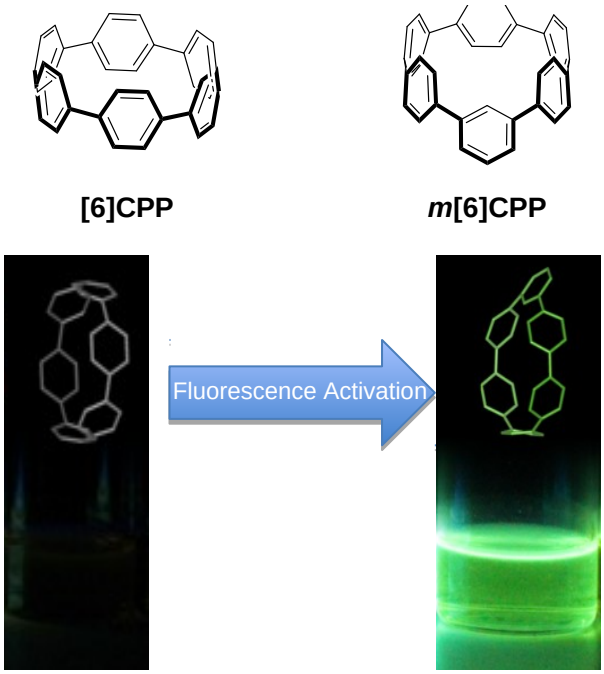

Figure 7. *Meta* Adjustment to CPPs[13]

In doing so, the symmetry of the nanohoop is broken allowing the smaller hoops to access fluorescent pathways that were previously restricted[13]. This adjustment is a key example of the tunability of CPPs and demonstrates how new properties can be unlocked by further manipulating the base nanohoop structure.

Furthermore, these nanohoops have been shown to be biocompatible. Introduction of compound **3** to living cells produced bright fluorescent images and the nanohoop was non-cytotoxic (not harmful to the cell). Additionally, this nanohoop was chemically stable in a biological context, unlike some of the common scaffolds mentioned above (Figure 8)[16].

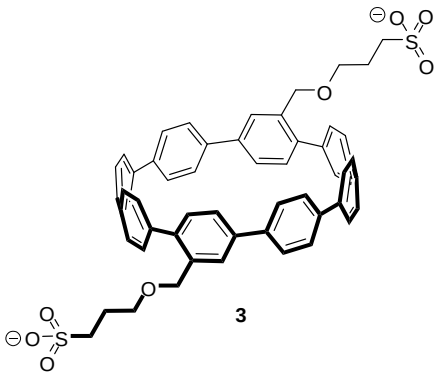

Figure 8. Sulfonated [8]CPP

Over the past several years, the Jasti lab has made significant developments in adapting the CPP structure and its photophysical properties to better function in biological imaging applications. Further research is needed to find ways to access red-shifted emission as well as improve the attachment of nanohoops to biomolecules.

Chapter II. The Road to a Red Nanohoop

II.I Introduction

Red-emitting fluorophores present their own unique advantages and shortcomings. Unlike other wavelengths of light, most biological materials do not emit light when they are excited with red light. This makes autofluorescence interference minimal when using red-emitting fluorophores, which increases the signal to noise ratio. Additionally, red light can penetrate tissue samples more effectively allowing deep tissue imaging with red fluorophores[6]. Therefore red-emitting fluorophores highly sought after.

Upon initially reviewing the wavelength trends of CPPs, one might assume that a red-emitting CPP could be made simply by synthesizing a small hoop. However, strain restrictions make that strategy impossible. As the number of rings within the hoop decreases, those rings are forced to bend to a greater degree creating strain that is eventually too unstable for the structure to be formed. Therefore, alternative approaches have to be taken. A widely used approach is the incorporation of electron donating and withdrawing moieties.

Installation of electron withdrawing group into a **[10]CPP** nanohoop structure caused a red-shift in emission relative to the parent molecule (**[10]CPTcaq**, Figure 9)[17].

This caused the HOMO-LUMO gap to narrow resulting in a red-shifting of the fluorescence.

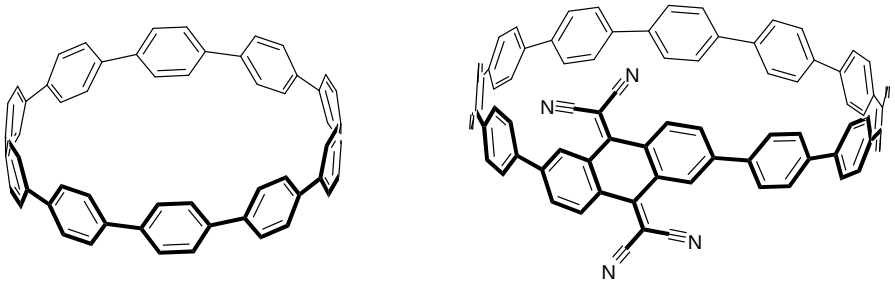

[10]CPP
λ_{em}: 466 nm
ϕ: 0.65

[10]CPTcaq
λ_{em}: 642 nm
ϕ: 0.05

Figure 9. **[10]CPP** and **[10]CPTcaq**

Unfortunately, this shift in fluorescence came at the cost of a low quantum yield and therefore, a low brightness. Another electron accepting unit that has been widely employed to red-shift fluorescence is the benzothiadiazole (BT) moiety (Figure 10). The BT moiety has been widely used to red-shift emission in conjugated polymers[18].

Benzothiadiazole Moitey

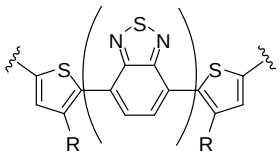

Figure 10. BT embedded polymer[18]

II.II Synthesis

The structure of the BT unit can be easily installed using standard CPP synthesis. **4a** is coupled with commercially obtained 4,7-Dibromobenzo[c]-1,2,5-thiadiazole in a Suzuki cross coupling to afford **4b** in 34% yield. **4b** is then deprotected followed by reductive aromatization to form **BT[10]CPP** as shown in Figure 11.

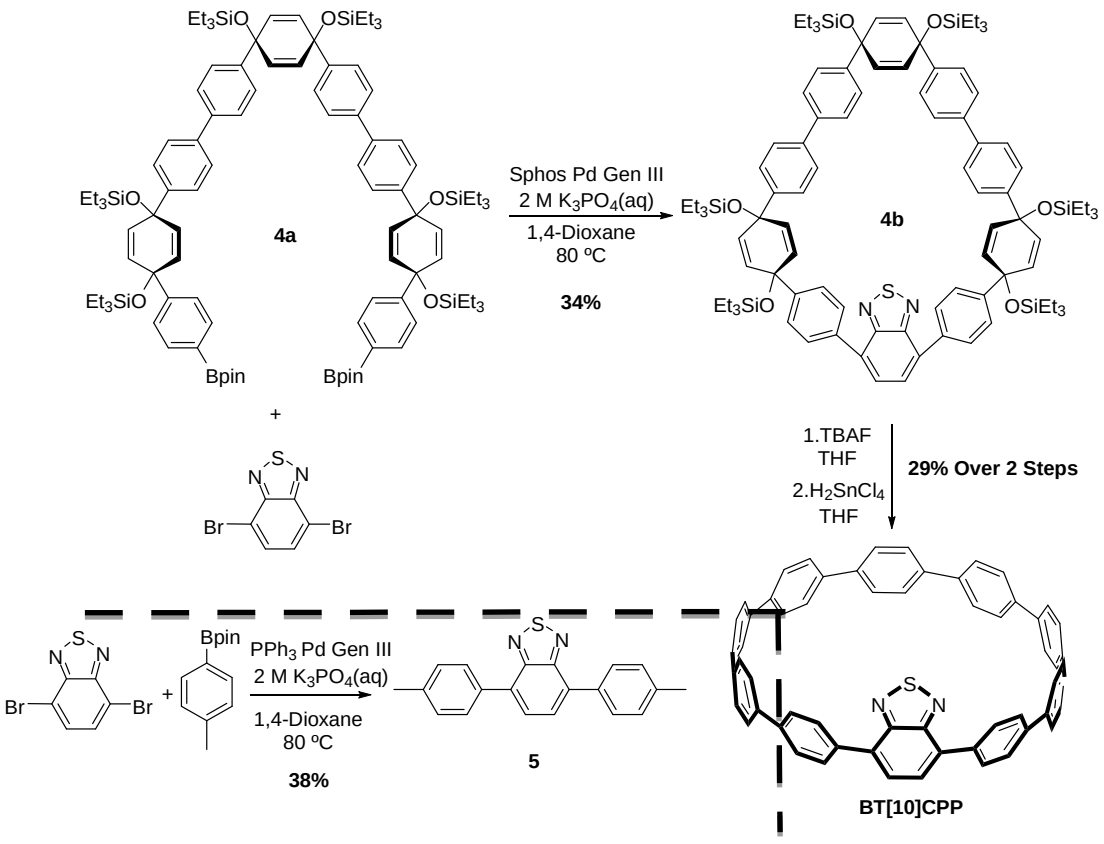

Figure 11. Synthetic Scheme of **BT[10]CPP**

A linear BT system (**5**) was synthesized for photophysical comparison by coupling 4,7-Dibromobenzo[c]-1,2,5-thiadiazole and 4,4,5,5-Tetramethyl-2-(*p*-tolyl)-1,3,2-dioxaborolane using Suzuki cross coupling conditions.

Following the success with the synthesis of **BT[10]CPP**, we wanted to determine if the size of the hoop could be decreased, which should yield a further red-shifted molecule. The same synthetic route used to make **BT[10]CPP** was used in an attempt to make **BT[8]CPP**. **6a** was coupled to commercially obtained 2,1,3-Benzothiadiazole-4,7-bis(boronic acid pinacol ester) using Suzuki cross coupling conditions to yield **6b**. Synthesis of the **6b** was successful although decomposition was observed. This finding suggests that the installation of the BT unit introduces instability restricting the size of hoop that can be made. An attempt to deprotect and aromatize **6b**

using H_2SnCl_4 were unsuccessful. During the aromatization reaction of this molecule a deep red color was observed, which quickly changed to orange. This color change may indicate formation of the desired **BT[8]CPP**, followed by rapid rearrangement.

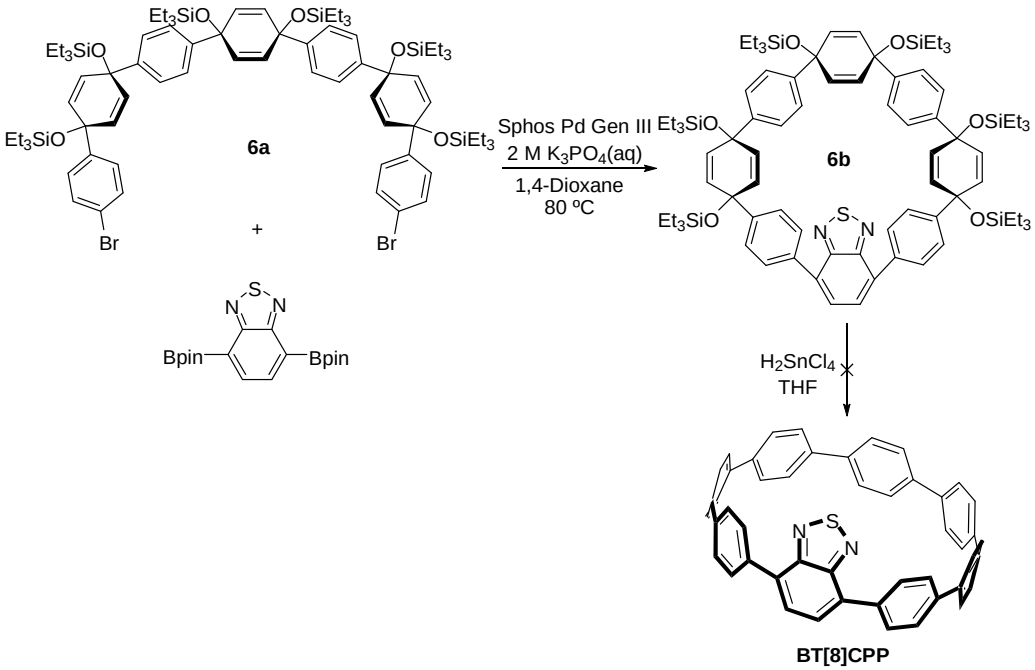

Figure 12. Synthetic Scheme of BT[8]CPP

Synthesis of **BT[10]CPP** and was confirmed via NMR, mass spectroscopy, and infrared spectroscopy (see materials and methods).

II.III Results

As hypothesized, the introduction of BT moiety into the nanohoop resulted in the shifting of the emission wavelength from 466 nm (**[10]CPP**) to 571 nm. Visually, the emission profile went from blue to orange. An even more dramatic shift is seen when comparing the linear benzothiadiazole analogue **5**. The significant increase in emission wavelength from **5** and **BT[10]CPP** indicates that the BT moiety alone is not sufficient for red shifting, and that curvature of the molecule is necessary to shift the emission further red.

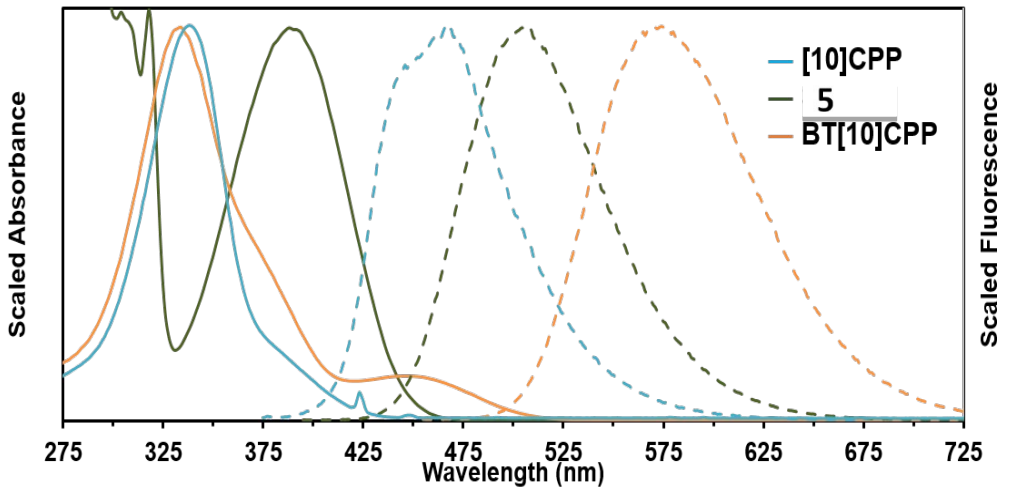

Figure 13. Emission Profile of **[10]CPP**, **BT[10]CPP**, and **5**

One unexpected discovery that came about when analyzing the fluorescence properties of **BT[10]CPP** was that the quantum yield did not decrease dramatically. This trend contradicts the standard trend observed for red-shifted fluorophores. Collaborator Terri Lovell proved that this is a result of the lack of intermolecular charge transfer.

Cyclic voltammetry (CV) was used to experimentally analyze the HOMO and LUMO levels. The results show an oxidation potential of 0.7838 V for **BT[10]CPP**. Conversely, the linear BT system had an oxidation potential of 1.145 V and a reduction potential of -1.989 V for the linear BT system (see Cyclic Voltammetry) . The decrease in oxidation potential suggests that the curvature of the BT unit within the aromatic chain causes the HOMO to be raised. This causes the HOMO-LUMO gap to shrink causing the observed red-shifting.[19]

One unique feature of **[10]CPP** that distinguishes it from the smaller hoops is its ability to act as a host for the spherical molecule C_{60}, or fullerene, as shown in Figure 14. This interaction causes a complete sequestration of **[10]CPP** fluorescence[20].

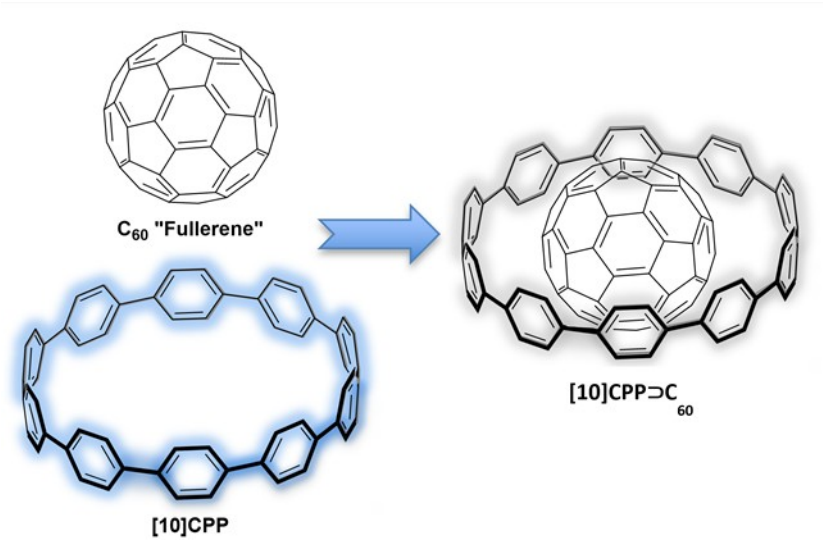

Figure 14. Host/Guest Interaction between **[10]CPP** and C_{60}

Using the changes in fluorescence intensity, the host/guest interaction can be quantified as a binding constant. A previous study[20] determined the binding constant for **[10]CPP**⊃C_{60} to be (2.79 ±0.03)x10^6. The same analysis was performed on **BT[10]CPP** to determine whether the installation of the BT moiety impacted the host properties of the nanohoop structure. Analysis of the host/guest interaction revealed that **BT[10]CPP** has a binding constant of (2.06±0.08)x10^6, which is within the range of that reported for **[10]CPP**. Figure 15 shows the gradual decrease in fluorescence intensity as the concentration of C_{60} increased.

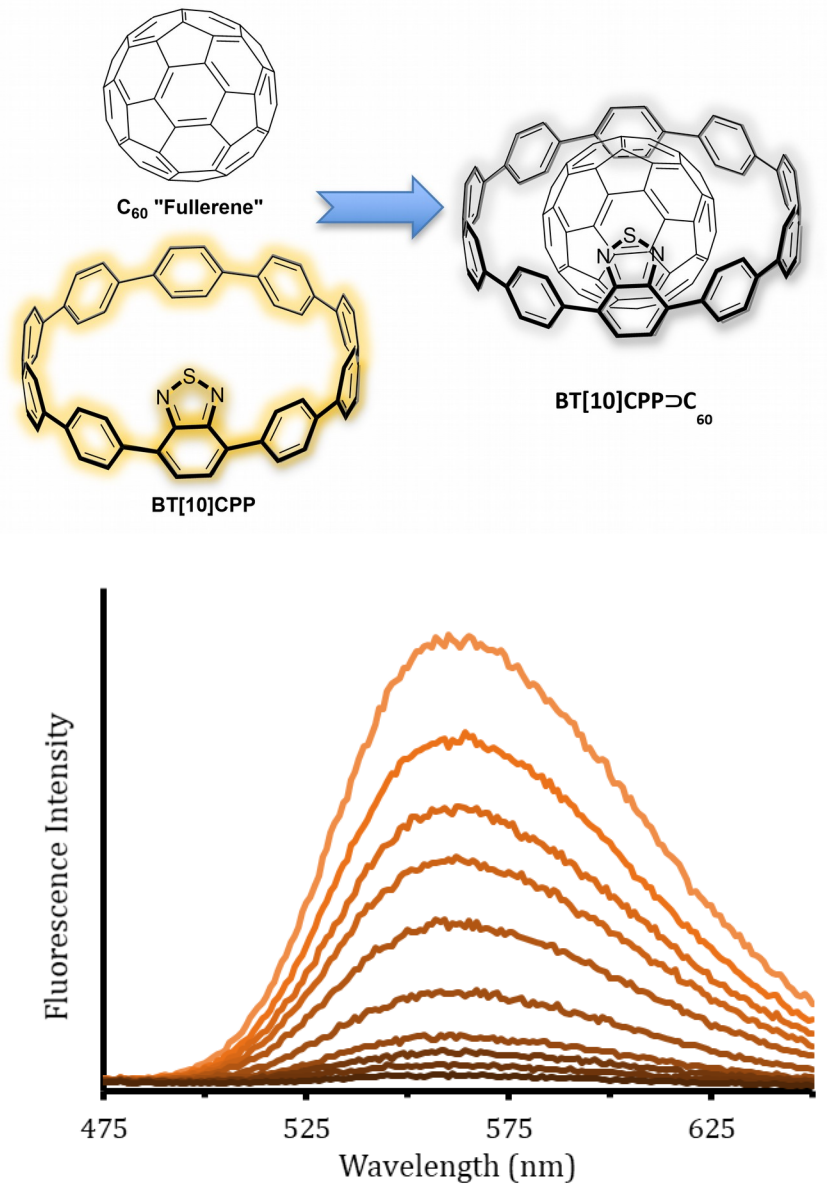

Figure 15. Host/Guest Analysis of **BT[10]CPP**

II.IV Conclusions/Future Directions

Analysis of **BT[10]CPP** revealed that incorporation of the BT unit into the **[10]CPP** scaffold resulted in a significant red-shifting in its emission profile. We were surprised to find that this red-shifting was not accompanied by reduction of quantum yield observed with other red-shifted fluorophores. This phenomenon appears to be due to a lack of intermolecular charge transfer which is present in other red-shifted

nanohoops like **[10]CPTcaq**. Further research is needed to explore the effects of installing other electron withdrawing moieties into CPPs. Additionally, BT moieties could be inserted to larger CPP hoops potentially unlock new colors. The initial success observed with **BT[10]CPP** have opened the doors for designing new bright red-shifted CPPs for fluorophore applications. This work is detailed in a submitted manuscript (Lovell, T. C.; Garrison, Z. R.; Jasti, R *Synthesis, characterization and computational investigation of bright orange-emittin benzothiadiazole [10]cycloparaphenylene*).

Chapter III. Sulfonation

III.I Introduction

While discoveries into unlocking new features and colors for CPPs have come a long way in the past several years, one of the largest hurdles left to clear in adapting CPPs for use as fluorophores is improving their attachment to biomolecules (conjugation or bioconjugation).

Many important fluorophore applications require attachment to biomolecules. One method to conjugate CPPs to DNA is through connection of an N-Hydroxysuccinimide (NHS) ester CPP with amine modified DNA. Unfortunately, preliminary tests of the conjugation capabilities of **7** demonstrated poor conjugation.

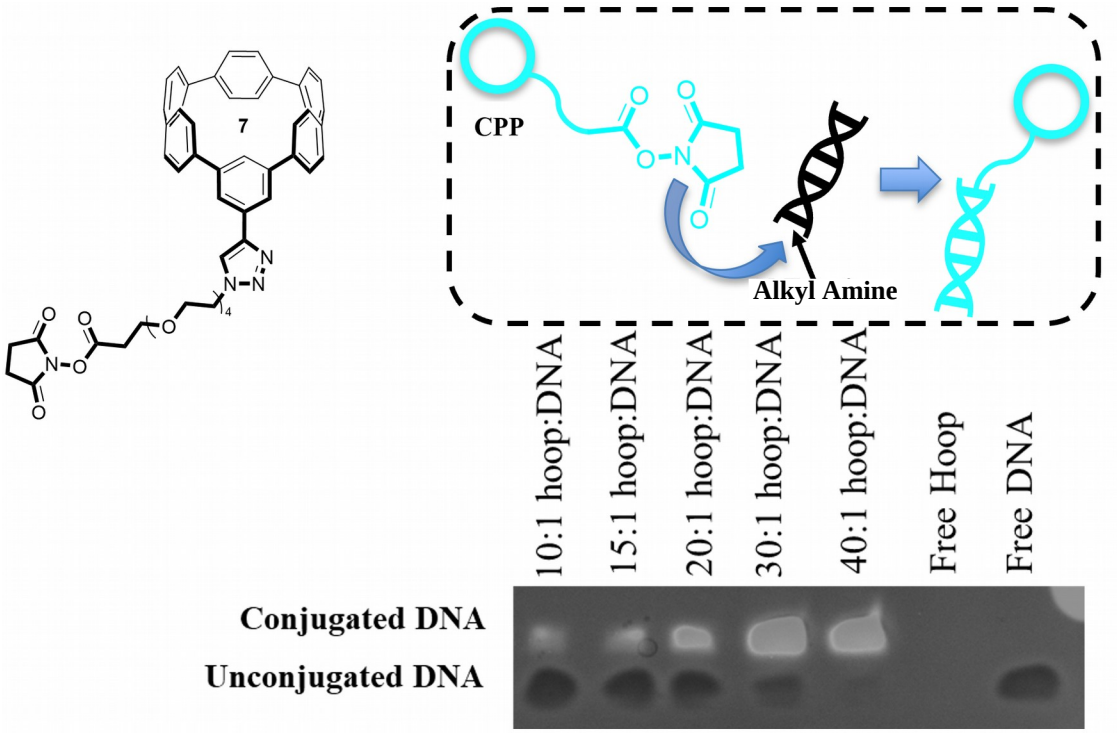

Figure 16. DNA conjugation testing of compound 7

As seen in Figure 16, the stains of conjugated DNA are relatively faint compared to unconjugated DNA when the ratio of hoop to DNA is low. This indicates that a majority of the DNA in solution remains unconjugated when exposed to CPP. The gel also reveals that a significant portion of DNA remains unconjugated until the concentration of **7** becomes exceedingly high (30:1 hoop to DNA). These results suggest that the CPP structure is ineffective in conjugating DNA and the structure requires further modification to improve its conjugation capabilities.

One potential way to improve conjugation for fluorophore structures is to install sulfonate functional groups. Addition of sulfonate groups to other fluorescent scaffolds such as fluorescein and coumarin greatly improved solubility and conjugation ability without hampering their fluorescent properties[21]. There are various synthetic routes to sulfonation, but the most commonly used method involves boiling acid, which is both

dangerous and low yielding. Therefore, it would be advantageous to explore other routes that involve less caustic conditions. We explored sulfonation through alcohol substitution, Grubbs metathesis, and nucleophilic addition of halides. These methods were explored with CPP building blocks to determine the most efficient sulfonation route for sulfonation of the CPP structure.

III.II Synthesis

The first route explored was using alcohols to attach sulfonates to the nanohoop (Figure 17). This route closely resembled the approach used previously to synthesize a sulfonated CPP[16]. The first step involves coupling **8a** to **8b** using Suzuki cross coupling conditions to yield the macrocycle **8c**. This coupling was extremely low yielding indicating that this approach would not be efficient if increased in scale. An additional complication is the unintentional deprotection of the tert-butyl(dimethyl)silyl (TBS) protected alcohols on **8a** which complicated purification of **8c**. The macrocycle is then deprotected with tetra-*n*-butylammonium fluoride (TBAF) and aromatized with H_2SnCl_4 to yield the diol-CPP: **8d**. The final step of the synthetic scheme is to perform a nucleophilic addition to attach a sulfonated carbon chain to the free alcohols on **8d** to yield **8e**. Due to the previously outlined issues, this synthetic scheme was abandoned.

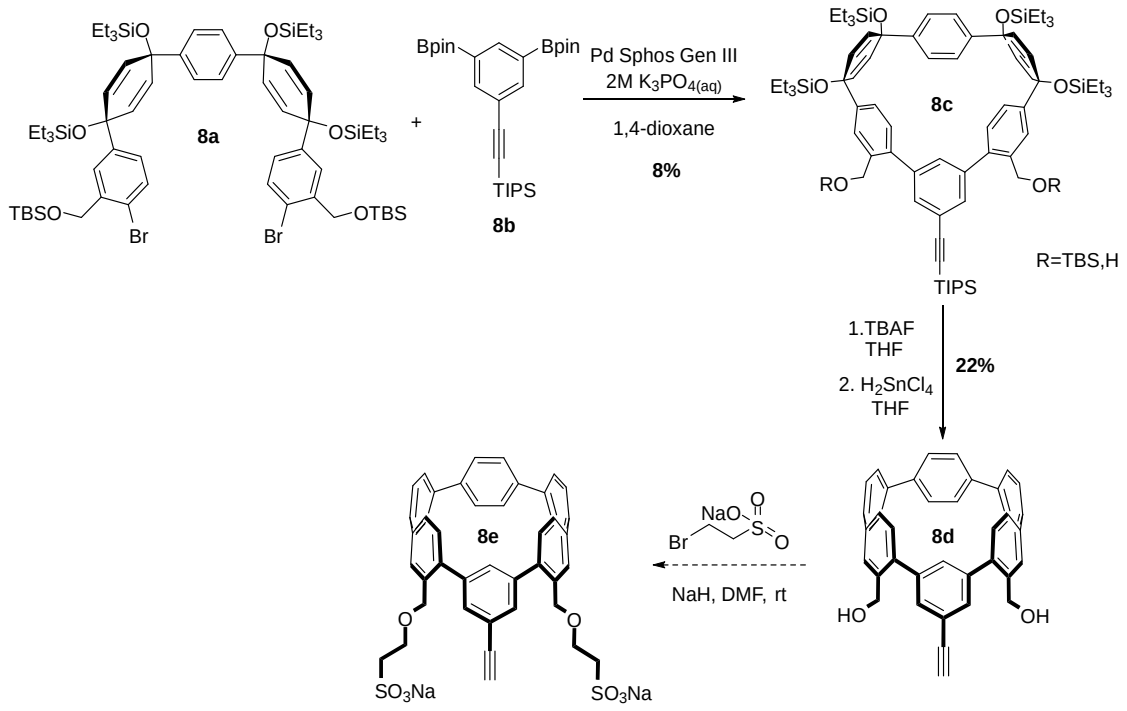

Figure 17. Sulfonation Scheme 1

The next approach utilized Grubbs metathesis to attach sulfonates. Previous research has shown that alkenes required for Grubbs metathesis can be carried through the CPP synthesis in high yields[22]. The route begins by converting 5-bromo-2-chlorotoluene to the brominated structure **9a** using N-bromosuccinimide (NBS) and benzoyl peroxide (BPO). A terminal alkene is then attached to **9a** forming **9b** using vinyl magnesium bromide and a lithium/halogen exchange. Purification of this reaction was extremely slow and low yielding creating a significant setback. The final step involves coupling **9b** to sulfonate **9c** via Grubbs metathesis to form **9d**. Unfortunately, attempts to metathesize these compounds were unsuccessful. Because **9c** contains a sulfonate functional group, it is very insoluble in organic solvents. This made its dissociation into the dichloromethane (DCM) solvent very poor and explains the poor outcome of the reaction. An alternative set of conditions using methanol as the solvent instead of DCM were also tested. Despite the improved dissociation of **9c**, **9b** displayed poor solubility

in methanol resulting in a failed reaction. These issues led us to abandon this synthetic scheme.

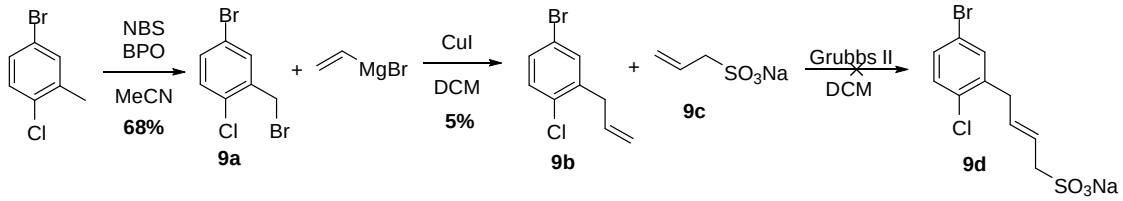

Figure 18. Sulfonation Scheme 2

The last synthetic scheme studied involved using a nucleophilic addition to a chloride. Reduction of 5-bromo-2-chlorotoluene using a borane dimethyl sulfide affords **10a**. This was followed by a chlorination using concentrated hydrochloric acid (HCl) to give **10b**. The final sulfonation step involves a refluxing **10b** with sodium sulfite in water to make **10c**.

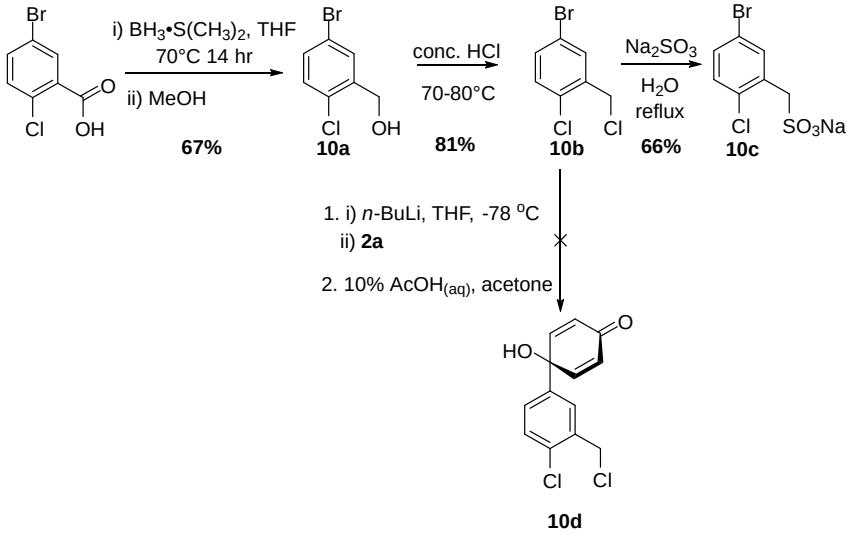

Figure 19. Sulfonation Scheme 3

The initial steps in the synthesis all proved to work effectively and compounds **10a-b** were all synthesized in high yields. The sulfonation step also appeared to work well and **10c** structure was confirmed via ^{1}H NMR and IR. The success of these reactions led us to pursue a sulfonated CPP using this method. Unfortunately, attempts

to lithiate **10b** were unsuccessful due to unintended lithiation at the added benzyl chloride instead of the bromide. This suggests that the benzyl chloride is too reactive to carry through multiple rounds of lithiation additions.

To decrease the reactivity of the chloride it was moved further away from the benzene ring. The route beings with the same bromination of 5-bromo-2-chlorotoluene to form **9a** as in Scheme 2. **9a** is then converted to form a phosphonium ion (**11a**) using triphenylphosphine. The phosphonium ion in **11a** is then reduced to a terminal alkene to using paraformaldehyde and potassium tert-butoxide to form **11b**. The terminal alkene can then be converted to a terminal alcohol in a hydroboration-oxidation reaction using borane dimethyl sulfide reagent followed by 1M NaOH, peroxide, and methanol to afford **11c**. **11c** can then be chlorinated using trimethyl silyl chloride to form **11d** which could be used as the central building block for building a CPP. Unfortunately, attempts to lithiate **11d** were unsuccessful. However, with further optimization of reaction conditions it might be possible to make **11e**.

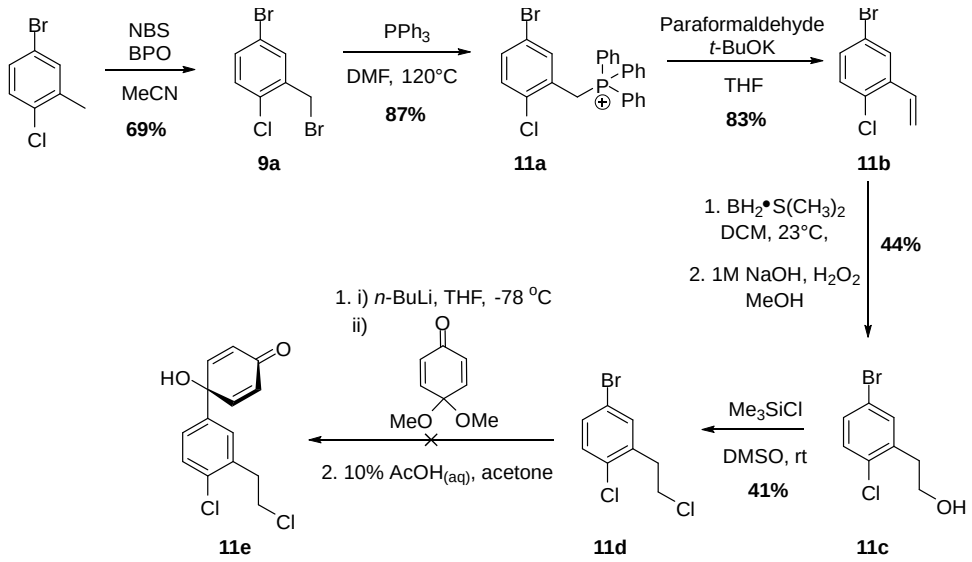

Figure 20. Sulfonation Scheme 4

III.III Conclusion/Future Directions

Difficulties with directly sulfonating the phenyl rings of the nanohoop suggest an alternative strategy is needed. One alternative method is to sulfonate the NHS-PEG (polyethylene glycol) linker and subsequently attach the sulfonated linker to the nanohoop as shown in Figure 21.

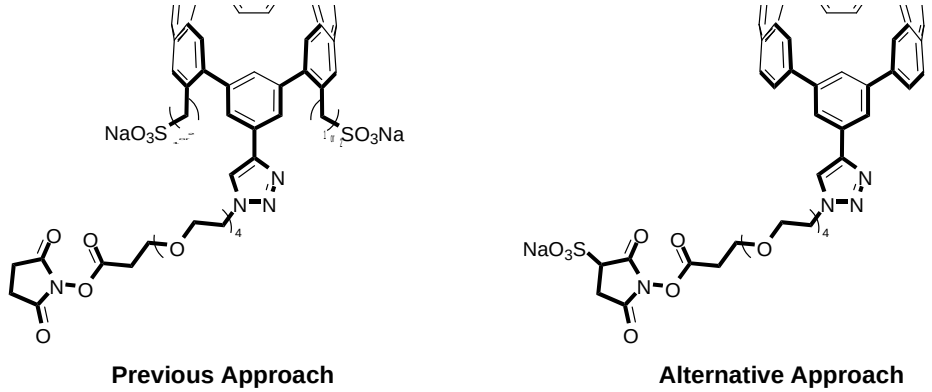

Figure 21. Alternative attachment of sulfonate group

This method would avoid issues that come with modifying the base CPP structure while also not increasing the number of reactions needed to reach the final product.

Despite facing challenges with these synthetic schemes, the various approaches have revealed important information about installing sulfonates into CPPs. Successful sulfonation of **10b** via nucleophilic addition of sodium sulfite could easily be adapted to simpler fluorophore scaffolds and may provide a much safer alternative to conventional methods. Further research is needed to identify a strategy that allows easy installation of sulfonates such that CPPs can be effectively bioconjugated and can be used in subsequent fluorophore applications.

Chapter IV. Materials and Methods

IV.I Overview

In order to synthesize the desired red shifted nanohoops, small curved building blocks were synthesized from basic commercially available materials. From these building blocks, larger pieces were assembled until a they could be linked together to make the desired macrocycle where it was characterized and studied. Synthesis of the sulfonated CPP components was done starting with similar starting materials to standard CPPs but with additional carbon branches to which the sulfonate group would be added. The intermediates of the final components were purified via extraction, filtration, flash chromatography, and size exclusion gel permeation chromatography. Structures were confirmed using ^{1}H NMR, ^{13}C NMR, mass spectrometry, and infrared spectroscopy.

IV.II Reaction Procedures

Unless otherwise stated, all of the following reactions were done in flame dried glassware (performed under vacuum) and kept under N_2 gas to avoid the accumulation of oxygen or water that could otherwise interrupt the reaction. All liquids were transferred using syringes and needles to minimize air contact while solid substances were transferred and then placed under vacuum before proceeding with the reaction.

Lithiation Addition

Halogen-Lithium exchange followed by nucleophilic addition into a ketone is one of the foundational reactions used to connect the rings together to form the nanohoop structure. The procedure for lithiation additions involves adding *n*-butyl

lithium to a solution of tetrahydrofuran (THF) and an aryl halide at -78 ºC. This is followed by the slow addition of the ketone substrate and stirring for 2 hours. The reaction is quenched with deionized water.

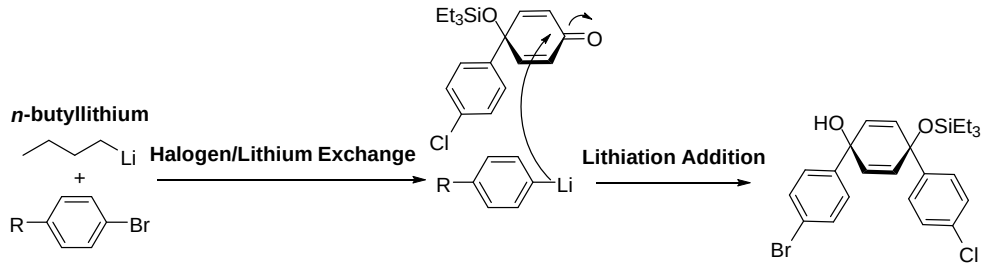

Figure 20. Lithiation Additions

“TES” Protection

The lithiation addition scheme outlined previously requires steric influence to form the curved orientation needed for nanohoop structure. TES groups are used to obtain stereoselective addition to one face of the molecule. The procedure for TES group implementation involves mixture of a hydroxyl containing structure with imidazole in dimethylformamide. Chlorotriethylsilane is then added to the solution and . left stirring overnight. The reaction quenched the following day using a saturated sodium bicarbonate solution.

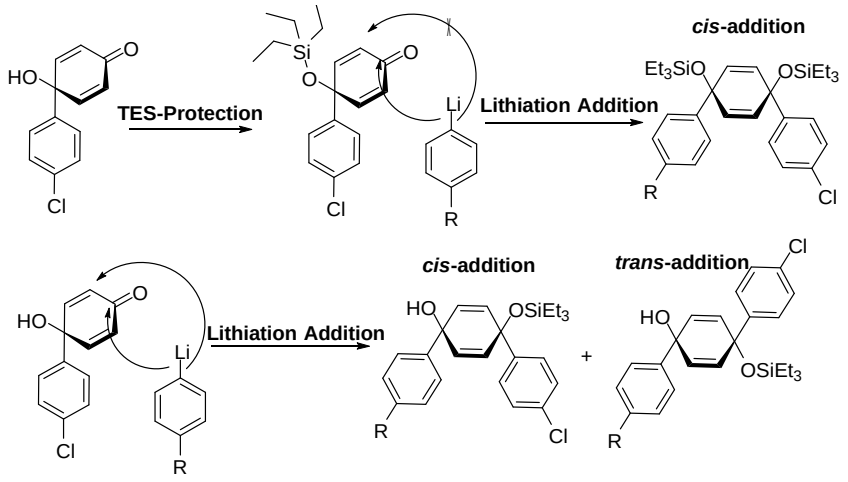

Figure 21. Stereoselective addition driven by steric hindrance of TES groups

Metal Catalyzed Reactions

The other reaction type used to link structures together are metal catalyzed reactions. The two used in this paper were Miyaura borylations and Suzuki cross coupling. Miyaura borylations require a palladium catalyst to replace a halogen (chlorine or bromine) with a bis(pinacolato)boronate (Bpin) group as shown below. The procedure for this reaction involves mixing the halide containing structure with $Pd(OAc)_2$, potassium acetate, and Bis(pinacolato)diboron in dioxane. The solution is heated to 80 ºC and left stirring overnight.

The other reaction that required a metal catalyst was Suzuki cross couplings. This reaction requires a different type of palladium catalyst to couple two carbons together, one attached to a halogen (usually chlorine) and the other attached to a Bpin group (Figure 22). The procedure for this reaction involves mixing the halogen containing structure with an excess of the Bpin containing structure along with

palladium triphenylphosphine gen III catalyst in dioxane. The solution is mixed and heated to 80 ºC before 2 molar potassium phosphate is added to the solution. The solution is stirred overnight.

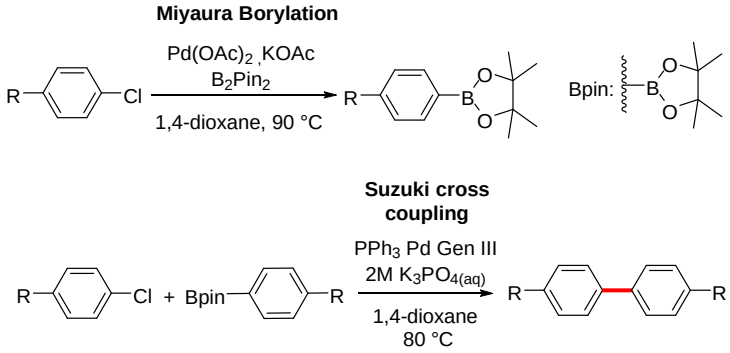

Figure 22. Metal Catalyzed Reactions

Macrocyclization

Macrocyclizations are a specific type of Suzuki cross coupling used to close the loop between two curved pieces. The major difference between the previously outlined Suzuki cross coupling is that the reaction conditions have to be altered to run in extremely dilute concentrations. This is done specifically so that intramolecular coupling (coupling within a single molecule) is favored as opposed to intermolecular coupling (coupling between two different molecules) as shown below:

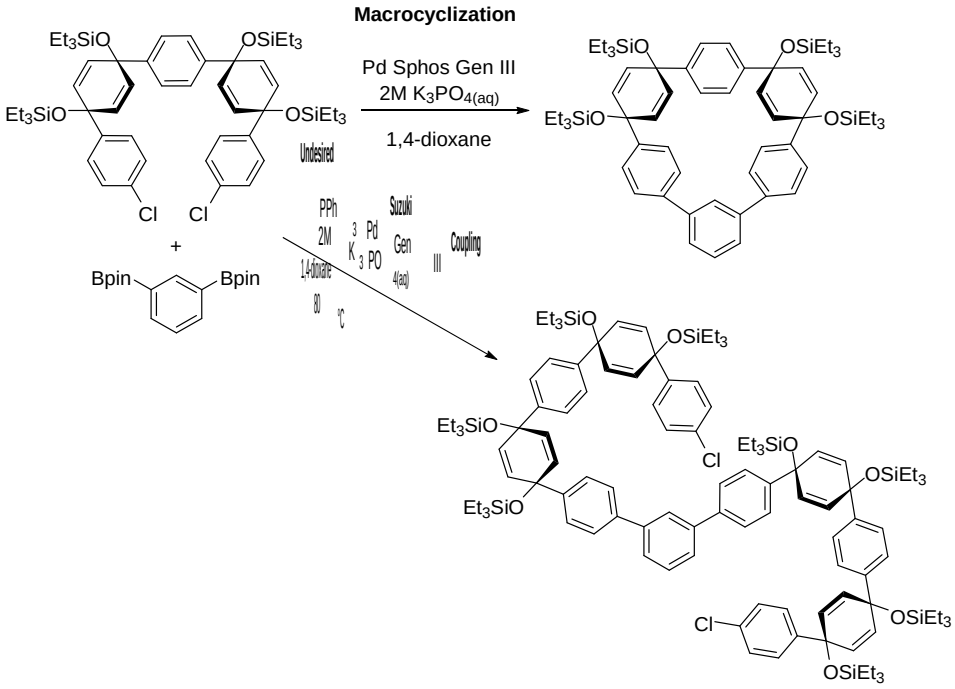

Figure 23. Macrocyclization vs. standard Suzuki coupling

Deprotection and Aromatization

The final step in the synthesis of a CPP is to fully aromatize the ring. Because several cyclohexadienes were used to facilitate the desired curvature in the molecules, there must be one last reaction to convert those rings into benzenes. The alcohols must first be deprotected using tert-butyl ammonium fluoride before they can be reduced. The aromatization reaction uses H_2SnCl_4 to facilitate the reduction of the rings. The procedure for this reaction involves mixing the macrocycle with a H_2SnCl_4 solution in THF at room temperature for an hour. The reaction is quenched with saturated sodium bicarbonate.

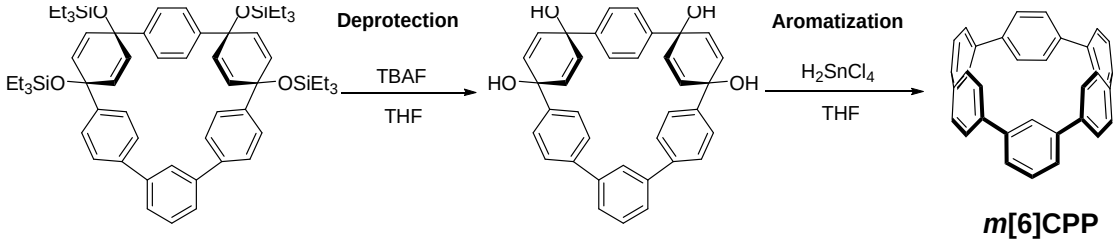

Figure 24. Deprotection and aromatization to form CPP

IV.III Purification

Liquid Extraction

Liquid extraction involves using different solubility preferences and solvent densities to separate the desired product from other materials. The standard extraction protocol involves having an aqueous (water) and organic (ethyl acetate, dichloromethane, etc.) solvent in a separatory funnel along with the reaction products. The synthesized organic products will be more soluble in the organic layer, while any aqueous soluble by-products or reactants will dissolve into the water layer. This technique requires subsequent vacuum concentration to remove the solvent for isolation of the dissolved product.

Precipitation

Precipitation involves putting the impure product into a solvent it is not soluble in. This will cause the product to crash out as a solid but ideally keep impurities in solution. The solid is then placed into a Büchner funnel and washed with the same solvent to remove all other impurities.

Flash Chromatography

Flash chromatography involves using the polarity of a molecule to separate it from other molecules of differing polarities. An impure mixture can be added to gel medium where it will be stuck until pushed through with a sufficiently polar solvent. Series of less polar solvents can be run through the gel medium collecting non-desired molecules. Automated flash chromatography was performed using a Biotage Isolera One

Gel permeation Chromatography

Similar to flash chromatography, an impure sample is purified by separating the individual components of the sample based on their properties. However, instead of separating the molecules based on polarity, gel permeation chromatography separates molecules by size. The sample is loaded onto a column filled with extremely small beads which trap smaller molecules and allow larger ones to pass through. This allows for a gradient to be formed with a range of molecule sizes which helps separate and purify a sample. Gel permeation Chromatography was performed using a Japan Analytical Industry LC-9101 preparative HPLC with JAIGEL1H/JAIGEL-2H columns in series using $CHCl_3$

IV.IV Characterization

NMR Spectroscopy

^{1}H (proton) NMRs were recorded at 500 or 600 MHz using a Varian INOVA-500 and Bruker Avance III-HD 500 or 600 spectrometer. ^{13}C (carbon) NMRs were recorded at 600 MHZ using Bruker Avance III-HD 600 spectrometer. NMR samples were dissolved in $CDCl_3$, $(CD_3)_2CO$, and D_2O.

Mass Spectroscopy

Mass spectrums were collected using the ASAP ionization technique on a Waters Xevo G2-XS QTof mass spectrometer.

Infrared Spectroscopy

Infrared absorption (IR) spectra were recorded on a Thermo Scientific Nicolet 6700 spectrometer equipped with a diamond crystal Smart ATR. Characteristic IR absorptions are reported in cm^{-1}

Host/Guest Binding Constant

Binding Constants were determined using fluorescence measurements in dichloromethane (DCM) using a a Horiba Jobin Yvon Fluoromax-4 Fluorimeter.

Cyclic Voltammetry

Cyclic Voltammetry experiments were performed using a Biologic SP-50 potentiostat with a Ag wire reference electrode, Pt wire counter electrode, and glassy carbon working electrode under nitrogen atmosphere in 100 mM solutions of Bu_4NPF_6 in dichloromethane (DCM) with ferrocene reference.

IV.V Materials

Substrate Reagents

Molecules were assembled using the listed commercially available starting materials or compounds provided from collaborators.

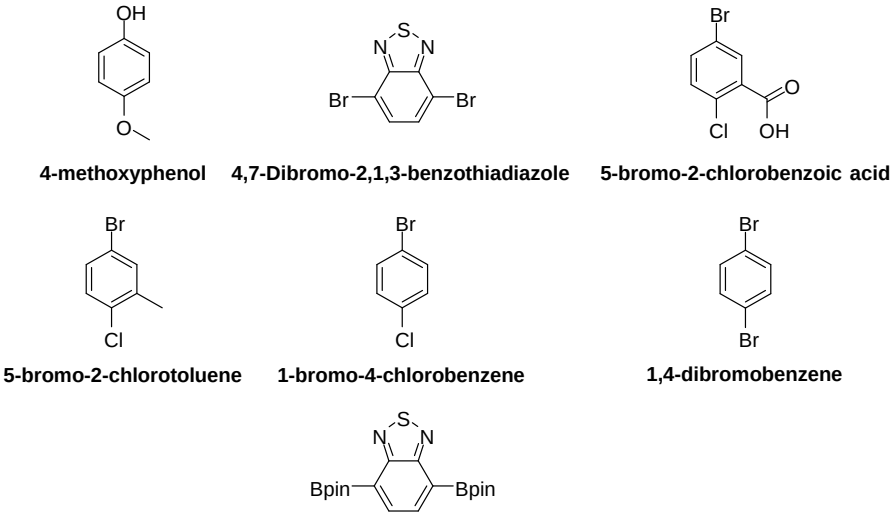

Figure 25. Substrate building blocks

Solvents

Reactions were run in Tetrahydrofuran (THF), dimethylformamide (DMF), dichoromethane, and 1,4-dioxane. Those solvents were stored in a PPT solvent purification system where they are run through a water-extraction column and stored under argon gas to maintain purity and absence of oxygen. Solvents not listed here were stored under air.

IV.VI Experimental Results

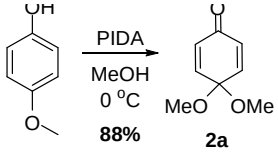

Synthesis of 2a. 4-methoxyphenol (100 g, 0.806 mol, 1 eq), and methanol (900 mL, 0.9 mol/L) was added to a 2 L flask with a stir bar. The flask was stirred in an ice bath at 0 ºC for 30 minutes. Phenyliodine diacetate (285 g, 0.806 mol, 1 eq) was slowly added to the flask over 45 minutes causing the solution to turn to a yellow/amber color. The flask was sealed under nitrogen and left stirring overnight at room temperature. The reaction was quenched with saturated sodium bicarbonate (50 mL) and extracted with dichloromethane (3 x 20 mL). The solution was washed with 2M NaOH (20 mL) followed by brine (20 mL). The solution was concentrated under vacuum yielding a red oil. The crude product was purified using a short-arm distillation setup at 45 ºC over several days yielding a yellow oil. The crude oil further purified via an alumina column (30% ethyl acetate/hexanes) to yield a light yellow oil (110.2 g, 88%). ^{1}H NMR (500 MHz, Chloroform-*d*) δ 6.83 (d, *J* = 10.3 Hz, 2H), 6.29 – 6.25 (m, 2H), 3.38 (s, 6H).

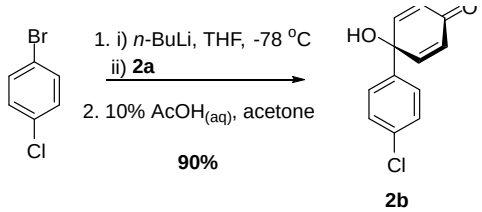

Synthesis of 2b. 1-bromo-4-chlorobenzene (13.66 g, 71.4 mmol, 1.1 eq) was added to a 250 mL round bottom flask with a stir bar and sealed under nitrogen. THF (102 mL, 0.7 mol/L) was added to the flask and the solution was stirred until all solid material had dissolved. The flask was placed into a dry ice bath at -78 ºC and left stirring for 30

minutes. *n*-butyl lithium (28.1 mL, 68.1 mmol, 1.05 eq) was added dropwise to the flask causing the solution to turn from clear to white. Immediately after all the *n*-butyl lithium was added, **2a** (8.7 mL, 64.9 mmol, 1 eq) was added to the flask dropwise. The flask was left stirring in the ice bath for an hour and then quenched with deionized water (10 mL). The product was extracted with ethyl acetate (3x 20 mL) and washed with brine (50 mL). The washed product was dried over sodium sulfate and concentrated under vacuum to yield a yellow solid. The solid was placed into a round bottom flask and dissolved in acetone (15 mL) and stirred while 10% acetic acid/water (15 mL) was added to the flask. The solution was stirred for an hour during which a pink solid formed. The reaction solution was quenched with saturated sodium bicarbonate (10 mL) and the formed precipitate was isolated using a Büchner funnel. The solid was washed with deionized water and saturated sodium bicarbonate solution yielding a white/light pink solid (12.84 g, 90%). ^{1}H NMR (500 MHz, Acetone-d_6) δ 7.56 (d, *J* = 8.7 Hz, 2H), 7.45 (d, *J* = 8.6 Hz, 2H), 6.95 (d, *J* = 10.1 Hz, 2H), 6.17 (d, *J* = 10.1 Hz, 2H), 2.85 (s, 1H).

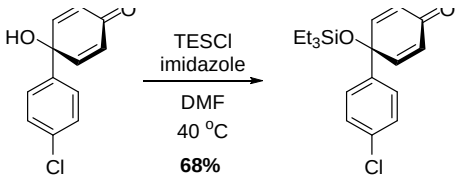

2b **2c**

Synthesis of 1c. **1b** (10.45 g, 47.4 mmol, 1 eq) and imidazole (12.89 g, 189 mmol, 4 eq) were added to a 500 mL round bottom flask with a stir bar. The flask was evacuated and then sealed under nitrogen. DMF (236 mL, 0.2 mol/L) was added to the flask and the solution was stirred until all solids had dissolved. Chlorotriethylsilane (9.54 mL, 56.8

mmol, 1.2 eq) was added to the flask and a venting needle was placed into the septa. The flask was left stirring overnight in an oil bath at 40 ºC. The flask was removed from the oil bath, unsealed, and quenched with saturated sodium bicarbonate (10 mL). The product was extracted with ethyl acetate (3 x 30 mL) and washed with 5% lithium chloride (LiCl) solution (3 x 20 mL). The washed crude product was dried over sodium sulfate and concentrated under vacuum to yield a dark yellow oil. The crude product was filtered through a silica gel plug and washed with hexanes (100 mL) followed by DCM (250 mL). The DCM wash was concentrated under vacuum yielding a light oil (10.85 g, 68%). ^{1}H NMR (500 MHz, Chloroform-*d*) δ 7.37 (d, *J* = 8.7 Hz, 2H), 7.31 (d, *J* = 8.7 Hz, 2H), 6.79 (d, *J* = 10.2 Hz, 2H), 6.23 (d, *J* = 10.0 Hz, 2H), 0.97 (t, *J* = 7.9 Hz, 12H), 0.69 – 0.63 (m, 8H).

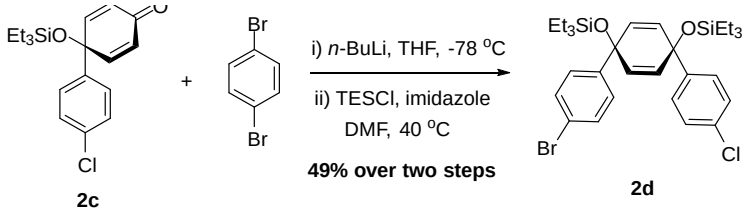

Synthesis of 2d. 1,4-dibromobenzene (3.8 g, 16.1 mmol, 1.58 eq) was added to a 250 mL round bottom flask with a stir bar and sealed under nitrogen. THF (20 mL, 0.7 mol/ L) was added to the flask and the solution was stirred until all the oil had dissolved. The flask was then placed into a dry ice bath at -78 ºC and left stirring for 30 minutes. *n*-butyl lithium (4.26 mL, 10.7 mmol, 1.05 eq) was added dropwise to the flask causing the solution to turn from clear to yellow. Immediately after all the *n*-butyl lithium was added, **2c** (3 mL, 10.2 mmol, 1 eq) was added to the flask dropwise. The flask was left stirring in the ice bath for an hour and then quenched with deionized water (10 mL).

The product was extracted with ethyl acetate (3x 20 mL) and washed with brine (30 mL). The product was dried over sodium sulfate and concentrated under vacuum to yield a white solid. The solid was then added to a 250 mL round bottom flask with a stir bar and imidazole (3.25 g, 47.8 mmol, 4 eq) and sealed under nitrogen. DMF (60 mL, 0.2 mol/L) was added to the flask and the solution was stirred until all solids had dissolved. Chlorotriethylsilane (2.41 mL, 14.3 mmol, 1.2 eq) was added to the flask and the flask was left stirring overnight in an oil bath at 40 ºC. The reaction was quenched with saturated sodium bicarbonate (15 mL) and then extracted with ethyl acetate (3 x 20 mL) and washed with 5% LiCl (5 x 10 mL). The product was dried over sodium sulfate and concentrated under vacuum to yield a white/green solid. Minor impurities were removed via precipitation in ethanol followed by sonication. The crude precipitate was collected using a Büchner funnel and was lightly washed with ethanol (1 mL). The product was concentrated under vacuum (3.55 g, 49%). ^{1}H NMR (500 MHz, Chloroform-*d*) δ 7.38 (d, *J* = 8.5 Hz, 2H), 7.23 (s, 5H), 7.17 (d, *J* = 8.6 Hz, 2H), 5.95 (s, 3H), 0.95 – 0.90 (m, 20H), 0.59 (qd, *J* = 7.9, 2.1 Hz, 16H).

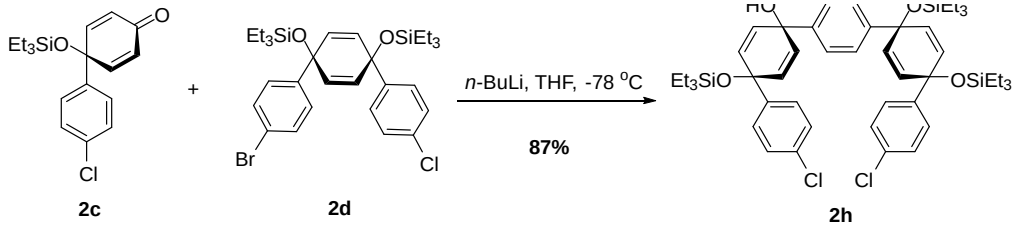

Synthesis of 2h. **2d** (4.98 g, 8.2 mmol, 1.1 eq) was added to a 50 mL round bottom flask with a stir bar and sealed under nitrogen. THF (10.6 mL, 0.7 mol/L) was added to the flask and the solution stirred until all solid material had dissolved. The flask was placed into a dry ice bath at -78 ºC and stirred for 25 minutes. *n*-butyl lithium (3.135

mL, 7.84 mmol, 1.05 eq) was added to the flask dropwise immediately followed by the addition of **2c** (1.9 mL, 7.46 mmol, 1 eq) dropwise. The flask was left stirring at -78 ºC for an hour. The reaction was quenched with deionized water (5 mL) and extracted with ethyl acetate (3 x 20 ml). The extracted product was washed with brine (30 mL) and then dried over sodium sulfate. The crude product was concentrated under vacuum yielding a light-yellow oil. The crude product was purified via silica flash chromatography (35% DCM/hexanes) yielding a white solid (5.61, 87%). ^{1}H NMR (500 MHz, Chloroform-*d*) δ 7.41 (d, *J* = 8.6 Hz, 3H), 7.36 – 7.34 (m, 5H), 7.25 (s, 3H), 7.20 (d, *J* = 8.6 Hz, 3H), 6.05 (d, *J* = 10.1 Hz, 4H), 5.96 (d, *J* = 10.1 Hz, 4H), 0.97 – 0.94 (m, 46H), 0.65 – 0.60 (m, 39H).

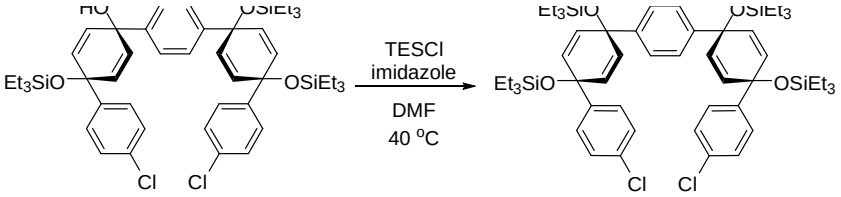

2h **2e**

Synthesis of 2e. **2h** (5.61 g, 6.5 mmol, 1 eq) and imidazole (1.77 g, 26.0 mmol, 4 eq) were added to a 100 mL round bottom flask with a stir bar. The flask was evacuated and then sealed under nitrogen. DMF (32.5 mL, 0.2 mol/L) was added to the flask and the solution was stirred until all solids had dissolved. Chlorotriethylsilane (2.4 mL, 14.3 mmol, 2.2 eq) was added and the flask was left stirring overnight in an oil bath at 40 ºC. The flask was removed from the oil bath, unsealed, and quenched with saturated sodium bicarbonate (10 mL). The product was extracted with ethyl acetate (3 x 10 mL) and washed with 5% LiCl (3 x 10 mL). The washed product was dried over sodium sulfate and concentrated under vacuum to yield a white solid (4.07 g, 64%). ^{1}H NMR (500

MHz, Chloroform-*d*) δ 7.23 (s, 1H), 7.20 (d, *J* = 7.2 Hz, 1H), 6.01 (d, *J* = 10.1 Hz, 1H), 5.91 (d, *J* = 10.2 Hz, 1H), 0.92 (dt, *J* = 15.8, 7.9 Hz, 9H), 0.62 (q, *J* = 7.9 Hz, 3H), 0.57 (q, *J* = 7.9 Hz, 3H).

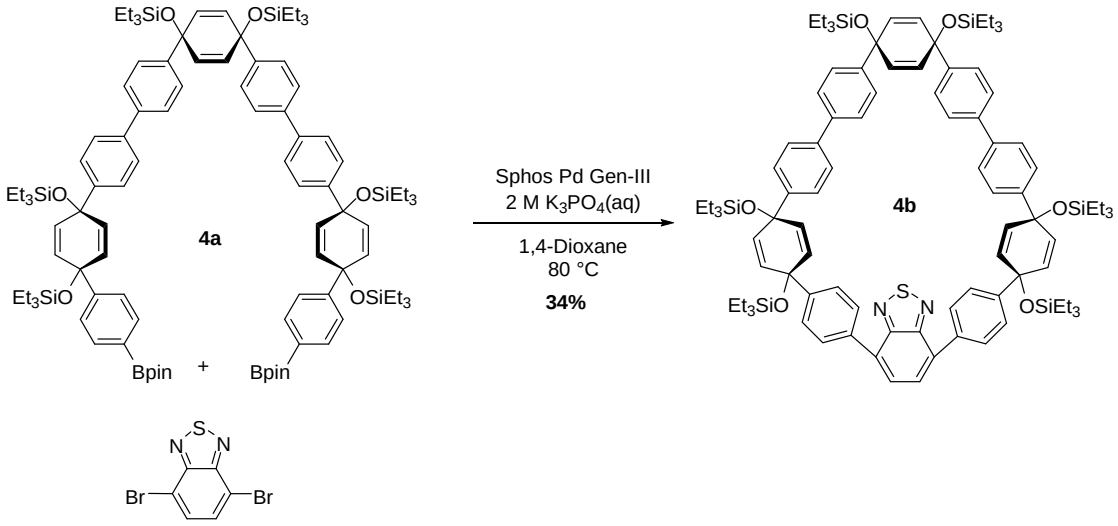

Synthesis 4b. 4,7-Dibromobenzo[c]-1,2,5-thiadiazole (0.065 g, 0.22 mmol, 1 eq), **4b** (0.4008 g, 0.23 mmol, 1.05 eq), and Sphos Pd Gen III (0.01398 g, 0.022 mmol) were added to a 250 mL round bottom flask with a stir bar. The flask was evacuated and backfilled with nitrogen (5x) before it was sealed under nitrogen. 1,4-dioxane and a solution of 2M K_3PO_4 were sparged separately for one hour. After one hour, 1,4-dioxane (69 mL, 0.003 mol/L) was transferred into the reaction flask and the solution was stirred and sparged with nitrogen gas for 20 minutes. The sparging needle was removed from the flask and the flask was placed into an oil bath and heated at 80 ºC for 10 minutes. Following heating, 2M K_3PO_4 (7.37 mL, 0.03 mol/L) was added to the flask and the solution was left stirring in the oil bath overnight. The reaction solution was filtered through a fritted funnel filled with celite and sodium sulfate. The funnel was washed with DCM. The collected wash was concentrated under vacuum to yield a dark

green/brown solid. The solid was purified via automated silica chromatography (0-60% DCM/hexanes). The purified product was concentrated under vacuum to yield a green solid (120 mg, 34%). ^{1}H NMR (500 MHz, Chloroform-d) δ 7.88 (d, J = 8.4 Hz, 4H), 7.78 (s, 2H), 7.51 (dd, J = 8.4, 3.2 Hz, 8H), 7.45 (d, J = 8.5 Hz, 8H), 7.32 (d, J = 8.4 Hz, 4H), 6.11 (d, J = 10.1 Hz, 4H), 6.02 (d, J = 10.1 Hz, 4H), 6.01 (s, 5H), 0.99 (td, J = 7.9, 5.8 Hz, 40H), 0.95– 0.89 (m, 33H), 0.68 (qd, J = 7.9, 3.6 Hz, 28H), 0.58 (q, J = 7.9 Hz, 19H). ^{13}C NMR (151 MHz, CDCl3) δ 154.07, 145.80, 145.59, 144.71, 139.42, 136.40, 132.91, 131.70, 131.54, 131.50, 128.90, 128.23, 126.72, 126.51, 126.47, 126.32, 126.16, 71.85, 71.80, 70.57, 7.10, 7.07, 6.54, 6.50, 6.47, 6.3. HRMS (ASAP) (m/z): [M+H] calculated for $C_{96}H_{128}N_2O_6SSi_6$, 1604.8109; found,1605.8112. IR (neat) 2951.83, 2909.21, 2879.98, 1488.82, 1456.90, 1412.99, 731.36 cm^{-1}

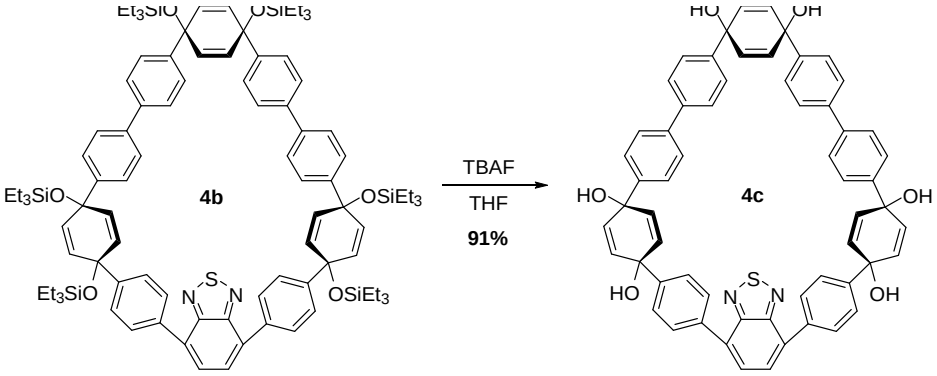

Synthesis of 4c. **4b** (0.121 g, 0.075 mmol, 1 eq) was dried under vacuum and then sealed under nitrogen in 10 mL scintillation vial with a stir bar. THF (0.753 mL, 0.1 mol/L) was added to the vial and the solution was stirred until all solid material had dissolved. Tetra-n-butylammonium fluoride (0.753 mL, 0.41 mmol, 10 eq) was added to the vial and left stirring for 1 hour. After an hour the reaction was quenched with deionized water (2 mL) causing a white precipitate to form. The precipitate was

isolated using a Büchner funnel and washed thoroughly with deionized water. The collected solid was dissolved in methanol and concentrated under vacuum yielding a green solid (63.1 mg, 91%).

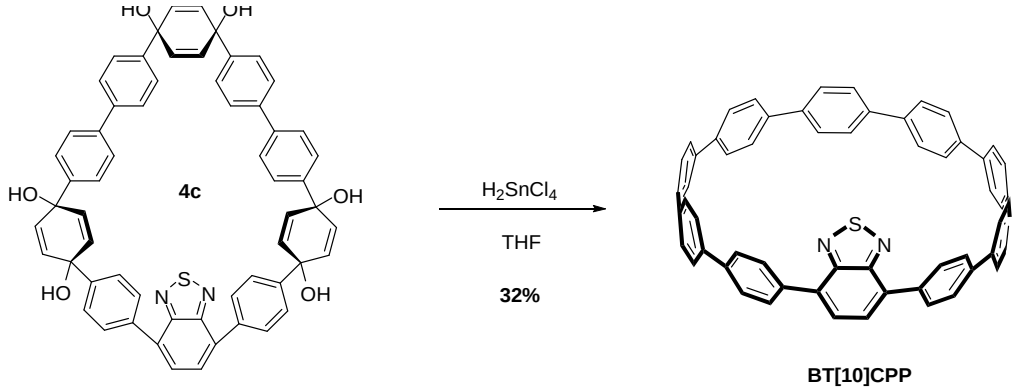

BT[10]CPP

Synthesis of BT[10]CPP. $SnCl_2 \bullet H_2O$ (0.1851 g) was added to a flame dried 100 mL round bottom flask with a stir bar and sealed under nitrogen. THF (20 mL) was added to the flask and the solution was stirred until all solid material had dissolved. Concentrated hydrochloric (HCl) acid (0.133 mL) was added to the flask and the solution was allowed to stir for 30 minutes. **4c** (63.1 mg) was placed in a 10 mL scintillation vial with a stir bar and sealed under nitrogen. H_2SnCl_4 (5.65 mL) was added to the scintillation vial and the solution was stirred for 1 hour during which the solution color transitioned from bright green to dark orange/yellow. The reaction was quenched with saturated sodium bicarbonate (1 mL) and the product was extracted with DCM (3 x 5 mL) and dried over sodium sulfate. The product was concentrated under vacuum and purified via gel permeation chromatography followed by alumina preparatory plate (100% DCM) yielding a bright orange solid (20 mg, 32%). ^{1}H NMR (600 MHz, Chloroform-*d*) δ 7.96 – 7.93 (m, 4H), 7.64 – 7.59 (m, 9H), 7.58 – 7.54 (m, 23H), 7.46 (s, 1H). ^{13}C NMR (126 MHz, CDCl3) δ 154.27, 139.62, 138.47, 138.24, 138.19, 138.17,

138.11, 137.84, 136.07, 130.95, 130.64, 128.11, 127.44, 127.40, 127.37, 127.34, 127.29, 127.08. HRMS (ASAP) (m/z): [M] calculated for $C_{60}H_{38}N_2S$, 818.2756; found, 818.2206. IR (neat) 2956.24, 2924.39, 2873.08, 2854.32, 1726.85, 1463.96, 738.43 cm^{-1}.

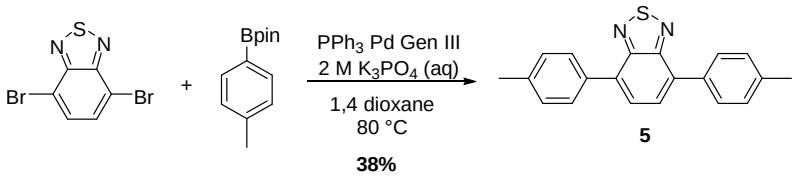

Synthesis of 5. 4,7-Dibromobenzo[c]-1,2,5-thiadiazole (0.14 g, 0.476 mmol, 1 eq), 4,4,5,5-Tetramethyl-2-(*p*-tolyl)-1,3,2-dioxaborolane (0.213g, 0.976 mmol, 2.05 eq, PPh_3 Pd Gen III catalyst (0.301 g, 0.048 mmol, 0.1 eq) were added to a flame dried 100 mL round bottom flask with a stir bar. The flask was evacuated and backfilled with nitrogen (5x) before it was sealed under nitrogen. 1,4-dioxane and a solution of 2M K_3PO_4 were sparged separately for one hour. After one hour, 1,4-dioxane (40 mL, 0.012 mol/L) was transferred into the reaction flask and the solution was stirred and sparged with nitrogen gas for 30 minutes. The sparging needle was removed from the flask and the flask was placed into an oil bath and heated at 80 ºC for 10 minutes. Following heating, 2M K_3PO_4 (15.9 mL, 0.03 mol/L) was added to the flask and the solution was stirred for a few minutes until the solution turned a dark green color. The reaction solution was filtered through a fritted funnel filled with celite and sodium sulfate. The funnel was washed with DCM and the collected solvent was concentrated under vacuum yielding a dark green/brown solid. The product was purified first by filtration through a silica gel plug followed by separate hexane and DCM washes. The collected DCM wash was then concentrated under vacuum and the isolated crude product was further purified using a

silica prep plate (50% DCM) yielding a bright green solid (57 mg, 38%). ^{1}H NMR (500 MHz, Chloroform-d) δ 7.84 (dd, J = 8.1, 1.6 Hz, 4H), 7.73 (s, 2H), 7.34 (d, J = 7.9 Hz, 4H), 2.44 (s, 6H). ^{13}C NMR (151 MHz, CDCl3) δ 154.23, 138.29, 134.66, 133.09, 129.38, 129.13, 127.79, 21.35. HRMS (ASAP) (m/z): [M+1] calculated for $C_{20}H_{16}N_2S$, 316.1034; found, 317.1112. IR (neat) 3027.17, 2915.53, 2360.21, 1907.44, 1610.56, 737.00 cm^{-1}.

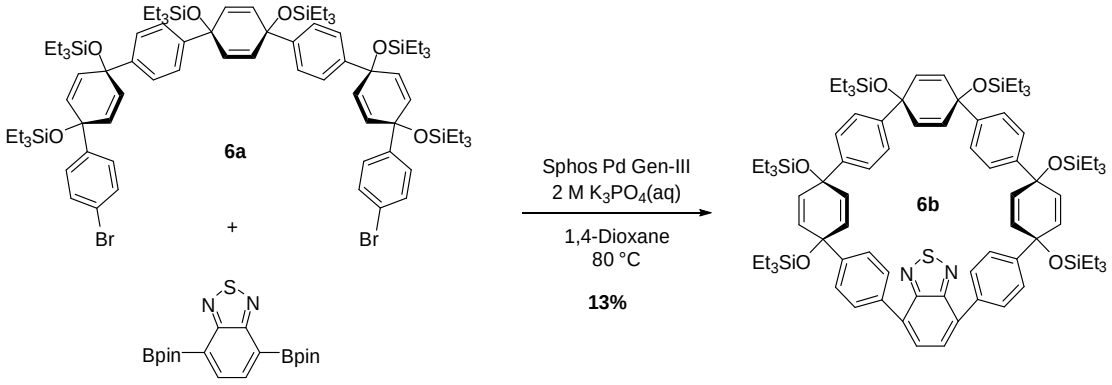

Synthesis of 6b. 2,1,3-Benzothiadiazole-4,7-bis(boronic acid pinacol ester) (0.067 g, 0.172, 1.05 eq), **6a** (0.243 g, 0.164 mmol, 1 eq), and Sphos Pd Gen III (0.013 g, 0.016 mmol, 0.1 eq) were added to a flame dried 500 mL round bottom flask with a stir bar. The flask was evacuated and backfilled with nitrogen (5x) before it was sealed under nitrogen. 1,4-dioxane and a solution of 2M K_3PO_4 were sparged separately for one hour. After one hour, 1,4-dioxane (54.7 mL, 0.003 mol/L) was transferred into the reaction flask and the solution was stirred and sparged with nitrogen gas for 20 minutes. The sparging needle was removed from the flask and the flask was placed into an oil bath and heated at 80 ºC for 10 minutes. Following heating, 2M K_3PO_4 (5.47 mL, 0.03 mol/L) was added to the flask and the solution was left stirring in the oil bath overnight. The reaction solution was filtered through a fritted funnel filled with celite and sodium

sulfate. The funnel was washed with DCM. The collected wash was concentrated under vacuum to yield a dark green/yellow solid. The solid was purified via automated silica chromatography (0-60% DCM/hexanes). The purified product was concentrated under vacuum to yield a green solid (30 mg, 13%). ^{1}H NMR (500 MHz, Chloroform-*d*) δ 7.77 (d, *J* = 8.3 Hz, 4H), 7.65 (s, 2H), 7.31 (d, *J* = 8.3 Hz, 4H), 7.14 (d, *J* = 8.1 Hz, 4H), 6.96 (d, *J* = 8.1 Hz, 4H), 6.06 (d, *J* = 10.0 Hz, 4H), 6.03 (s, 3H), 5.96 – 5.93 (m, 4H), 1.00 (t, *J* = 7.9 Hz, 20H), 0.91 (dt, *J* = 10.5, 7.9 Hz, 33H), 0.68 (q, *J* = 8.0 Hz, 17H), 0.62 – 0.55 (m, 22H), 0.51 (q, *J* = 8.0 Hz, 10H). ^{13}C NMR (151 MHz, CDCl3) δ 154.25, 145.98, 145.32, 144.08, 136.68, 133.31, 132.21, 132.10, 132.07, 131.84, 131.71, 131.60, 129.80, 129.19, 128.32, 128.09, 126.79, 126.71, 126.32, 126.26, 125.90, 125.78, 125.51, 125.24, 71.85, 71.82, 71.56, 71.51, 71.39, 69.50, 7.19, 7.08, 7.06, 7.02, 6.60, 6.58, 6.53, 6.50, 6.48, 6.47, 6.44, 6.34, 4.99.

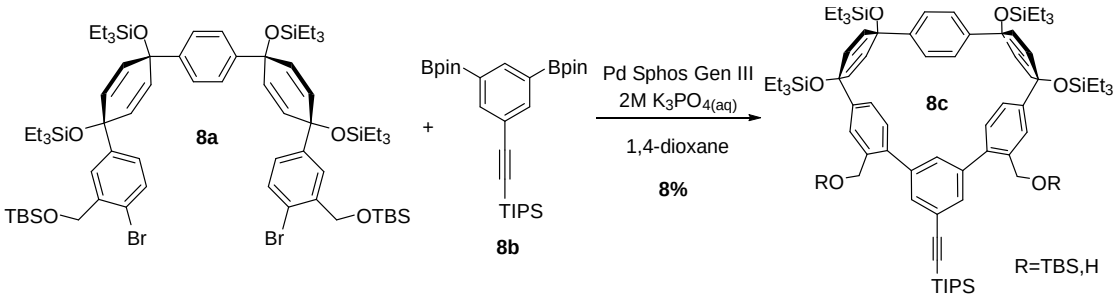

Synthesis of 8c. **8a** (0.5 g, 0.369 mmol, 1 eq), **8b** (0.198 g, 0.387 mmol, 1.05 eq), Sphos Pd Gen III (0.023 g, 23.3 mmol, 0.1 eq) were added to a flame dried 250 mL round bottom flask with a stir bar. The flask was evacuated and backfilled with nitrogen (5x) and then sealed under nitrogen. 1,4-dioxane and a solution of 2M K_3PO_4 were sparged separately for one hour. After one hour, 1,4-dioxane (115 mL, 0.003 mol/L) was transferred into the reaction flask and the solution was stirred and sparged with nitrogen

gas for 20 minutes. The sparging needle was removed from the flask and the flask was placed into an oil bath and heated at 80 ºC for 10 minutes. Following heating, 2M K_3PO_4 (12.3 mL, 0.03 mol/L) was added to the flask and the solution was left stirring in the oil bath overnight. The reaction solution was filtered through a fritted funnel filled with celite and sodium sulfate. The funnel was washed with DCM. The collected wash was concentrated under vacuum to yield a light red oil. The oil was purified via automated silica chromatography (0-50% DCM/hexanes) and the product was concentrated under vacuum to yield a clear oil (0.0451 g, 8%). The impure product was pushed forward to next reaction.

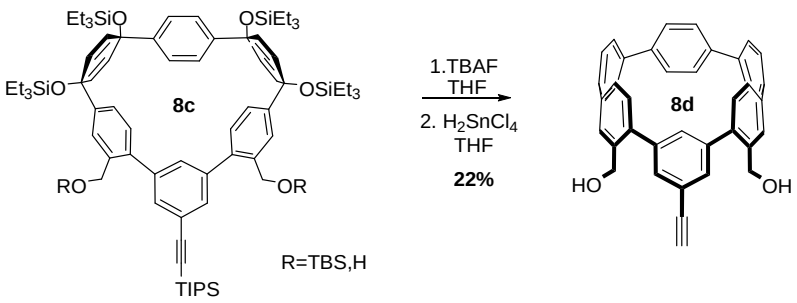

Synthesis of 8d. **8c** (0.0451 g, 0.031 mmol, 1 eq) was added to a 10 mL scintillation vial with a stir bar and sealed under nitrogen. THF (0.31 mL, 0.1 mol/L) was added to the scintillation vial and the solution was stirred until all of the **8c** material had dissolved. Tetra-n-butylammonium fluoride (0.31 mL, 0.31 mmol, 10 eq) was added to the scintillation vial and the solution was stirred for an hour. The reaction was quenched with 1 mL of deionized water causing a white precipitate to crash out of solution. The precipitate was isolated using a Büchner funnel and dried under vacuum before being sealed in a scintillation vial under nitrogen. $SnCl_2 \cdot H_2O$ (0.181 g, 0.8 mmol, 1 eq) was added to a flame dried 100 mL round bottom flask with a stir bar and sealed under

nitrogen. THF (20 mL, 0.04 mol/L) was added to the flask and the solution was stirred until all solid material had dissolved. Concentrated HCl acid (0.133 mL, 1.6 mmol, 2 eq) was added to the flask and the solution was allowed to stir for 30 minutes. H_2SnCl_4 (2.56 mL, 0.1 mmol, 3.3 eq) was added to the scintillation vial and the solution was stirred for 1 hour during which the solution color transitioned to a bright blue/green color. The reaction was quenched with saturated sodium bicarbonate (1.5 mL) and then extracted with DCM (3x). The product was dried over sodium sulfate and concentrated under vacuum to yield a yellow oil that fluoresced green. The oil was purified via alumina preparatory plate (3% methanol/DCM) yielding a clear oil that fluoresced blue (3.69 mg, 22%). ^{1}H NMR (600 MHz, Chloroform-*d*) δ 7.61 – 7.59 (m, 6H), 7.56 (d, *J* = 2.0 Hz, 0H), 7.55 (d, *J* = 2.0 Hz, 2H), 7.53 – 7.48 (m, 4H), 7.48 – 7.44 (m, 5H), 7.44 – 7.41 (m, 4H), 7.33 (dd, *J* = 8.4, 2.1 Hz, 3H), 5.47 (s, 1H), 5.41 (s, 1H), 4.41 (d, *J* = 8.7 Hz, 3H).

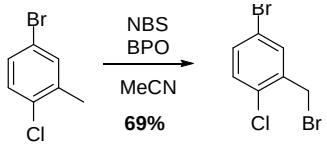

9a

Synthesis of 9a. 5-bromo-2-chlorotoluene (12.9 mL, 97.3 mmol, 1 eq), n-bromosuccinimide (19.06g, 107 mmol, 1.1 eq), benzoyl peroxide (0.471g, 1.94 mmol, 0.02 eq) acetonitrile (487 mL, 0.2 mol/L) were added to a flame dried 1 L round bottom flask with a stir bar. The solution was stirred until the solid materials had fully dissolved. A reflux condenser was attached to the flask and the solution was refluxed in an oil bath at 110 ºC overnight. Reaction progress was tracked via thin-layer chromatography (TLC) plating. Upon completion, the reflux condenser was removed

and sodium sulfite (4 g) was added to the flask. The solution was allowed to stir for a few minutes while the solution turned from a light-yellow color to almost clear. The crude product was extracted with DCM (3 x 30 mL) and washed with brine (40 mL) before it was concentrated under vacuum to yield a yellow solid. The solid was then recrystallized with methanol and isolated via suction filtration yielding a fluffy crystalline solid (18.7 g, 68%). ^{1}H NMR (500 MHz, Chloroform-*d*) δ 7.58 (d, *J* = 2.4 Hz, 1H), 7.38 (dd, *J* = 8.5, 2.4 Hz, 1H), 7.25 (s, 0H), 4.51 (s, 2H).

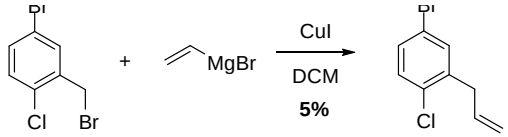

9a **9b**

Synthesis of 9b. **9a** (2.9868 g, 10.5 mmol, 1 eq) and copper iodide (1.001 g, 5.25 mmol, 0.5 eq) were added to a flame dried 250 mL round bottom flask with a stir bar. The flask was placed under vacuum and backfilled with nitrogen before being sealed with a septum. DCM (52 mL, 0.2 mol/L) was added to the flask and the solution was stirred until all of the solids had dissolved. The flask was then placed into a dry ice bath at -78 ºC and allowed to cool for 30 minutes. After the solution had cooled, vinyl magnesium bromide (22.1 mL, 22.0 mmol, 2.1 eq) was added to the flask dropwise over 15 minutes. Once all of the vinyl magnesium bromide had been added, the flask was left stirring in the dry ice bath for 3 hours. After 3 hours, the flask was removed from the ice bath and allowed to warm to room temperature during which the solution turned from a light-orange color to black. The reaction was quenched with saturated aqueous ammonium chloride (20 mL) and then filtered through a fritted funnel filled with celite. The funnel was washed with ethyl acetate and the collected wash was washed with

brine. The crude product was concentrated under vacuum to yield a mixture of white solid and yellow oil. The crude product was purified via vacuum distillation at 120 ºC for several hours. ^{1}H NMR (500 MHz, Chloroform-*d*) δ 7.36 (d, *J* = 2.4 Hz, 1H), 7.28 (dd, *J* = 8.5, 2.3 Hz, 1H), 7.22 (d, *J* = 8.5 Hz, 1H), 5.93 (ddt, *J* = 16.8, 10.0, 6.5 Hz, 1H), 5.18 – 5.04 (m, 2H), 3.49 – 3.42 (m, 2H).

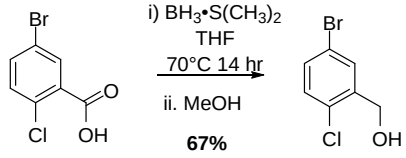

10a

Synthesis of 10a. 5-bromo-2-chlorobenzoic acid (5 g, 21.2 mmol, 1 eq) was added to a flame dried 100 mL flask with a stir bar and sealed under nitrogen. THF (53 mL, 0.4 mol/L) was added to the flask and the solution was stirred until all of the solid material had dissolved. The flask was then placed into an ice bath at 0 ºC and stirred for 30 minutes. After 30 minutes, borane dimethyl sulfide (5.05 mL, 53.1 mmol, 2.5 eq) was added to dropwise to the flask. The flask was left stirring for 15 minutes before a reflux condenser was attached and the flask was refluxed at 70 ºC overnight. The reaction was quenched with methanol (20 mL) and deionized water was used to crash out a white solid. The organic solvents were removed under vacuum and the solid was collected in a Büchner funnel and washed with deionized water and DCM. ^{1}H NMR (500 MHz, Chloroform-*d*) δ 7.67 (d, *J* = 2.4 Hz, 1H), 7.36 (dd, *J* = 8.4, 2.4 Hz, 1H), 7.22 (d, *J* = 8.5 Hz, 1H), 4.76 (d, *J* = 4.5 Hz, 2H), 1.96 (s, 1H).

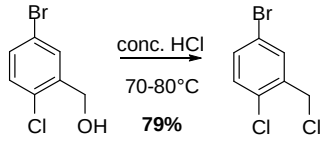

10a **10b**

Synthesis of 10b. **10a** (1 g, 4.51 mmol, 1 eq) was added to a flame dried round bottom flask with a stir bar. Concentrated HCl (137 mL, 0.033 mol/L) was added to the flask and the solution was allowed to stir for several minutes before it was sealed under nitrogen. The flask was placed into an oil bath at 80 ºC and left stirring overnight. The following day, the reaction was removed from the oil bath and placed into an ice bath at 0 ºC causing a white precipitate to crash out of solution. The solid product was isolated using a Büchner funnel. Additional product was collected from the reaction solution via extracting with DCM (3x). The extracted product was dried over sodium sulfate and concentrated under vacuum to yield the same white solid (0.855 g, 79%). ^{1}H NMR (500 MHz, Chloroform-*d*) δ 7.62 (d, *J* = 2.4 Hz, 1H), 7.40 (dd, *J* = 8.5, 2.4 Hz, 1H), 7.26 (d, *J* = 8.5 Hz, 1H), 4.64 (s, 2H).

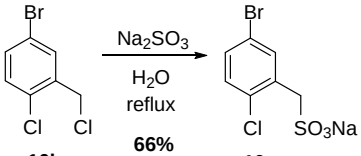

10b **10c**

Synthesis of 10c. **10b** (200 mg, 0.834 mmol, 1eq) and sodium sulfite (116 mg, 0.917 mmol, 1.1 eq) were added to a 25 mL round bottom flask with a stir bar. Deionized water (2.8 mL, 0.3 mol/L) was added to the flask and a reflux condenser was attached. The flask was stirred until all the sodium sulfite had dissolved and then refluxed at 110 ºC overnight. The following day, the flask was removed from the oil bath and allowed to acclimate to room temperature. The flask was then washed with DCM and the

remaining white solid was isolated using a Büchner funnel. The isolated product was dried under vacuum (0.0169g, 66%). ^{1}H NMR (500 MHz, Deuterium Oxide) δ 4.34 (d, *J* = 2.4 Hz, 1H), 4.17 (dd, *J* = 8.6, 2.5 Hz, 1H), 4.05 (d, *J* = 8.6 Hz, 1H), 1.01 (s, 2H).

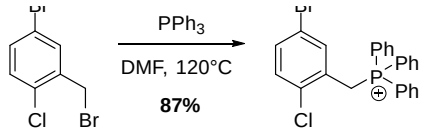

9a **11a**

Synthesis of 11a. **9a** (3.175 g, 11.2 mmol, 1 eq) and triphenylphosphine (7.32 g, 27.9 mmol, 2.5 eq) was added to a flame dried 100 mL round bottom flask with a stir bar. The flask was evacuated and backfilled with nitrogen (3x) and then sealed under nitrogen. DMF (44.7 mL, 0.25 mol/L) was added to the flask and the solution was stirred until all solids had dissolved. The flask was then placed into an oil bath and stirred at 150 ºC overnight. The following day the flask was removed from the oil bath and allowed to cool to room temperature. The reaction solution was then transferred to a new flask containing ethyl acetate (50 mL) causing a white precipitate to crash out of solution. The precipitate was isolated using a Büchner funnel and was lightly washed with hexanes. The isolated solid was dried under vacuum yielding clear white solid (4.54 g, 87%). ^{1}H NMR (500 MHz, Chloroform-*d*) δ 7.79 (ddd, *J* = 20.6, 10.5, 7.1 Hz, 9H), 7.66 (td, *J* = 7.8, 3.4 Hz, 6H), 7.58 (s, 1H), 7.34 (d, *J* = 8.6 Hz, 1H), 7.05 (d, *J* = 8.5 Hz, 1H), 5.73 (d, *J* = 14.6 Hz, 2H), 2.92 (d, *J* = 38.3 Hz, 1H), 1.77 (s, 2H).

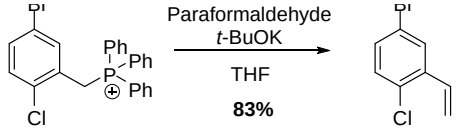

11a **11b**

Synthesis of 11b. **11a** (4.5 g, 9.64 mmol, 1 eq) was added to a flame dried 100 mL round bottom flask with a stir bar and placed under vacuum for a few minutes. THF (48.2, 0.2 mol/L) and paraformaldehyde (2.026 g, 67.5 mmol, 7eq) were added to the flask and the solution was stirred until all solid material had dissolved. Potassium tert-butoxide (2.16 g, 19.2 mmol, 2 eq) was slowly added to the flask to avoid overheating the solution. Addition of potassium tert-butoxide caused the solution to turn yellow which over time eventually faded to a clear white color. The flask was then sealed under nitrogen and left stirring at room temperature for 90 minutes. After 90 minutes, the reaction solution was filtered through a celite plug and washed with hexanes. The collected hexanes wash was concentrated under vacuum to yield a clear oil (1.75 g, 83%). ^{1}H NMR (500 MHz, Chloroform-*d*) δ 7.68 (d, *J* = 2.4 Hz, 1H), 7.31 (dd, *J* = 8.5, 2.4 Hz, 1H), 7.22 (d, *J* = 8.4 Hz, 1H), 7.01 (dd, *J* = 17.5, 11.0 Hz, 1H), 5.74 (d, *J* = 17.6 Hz, 1H), 5.43 (d, *J* = 11.0 Hz, 1H).

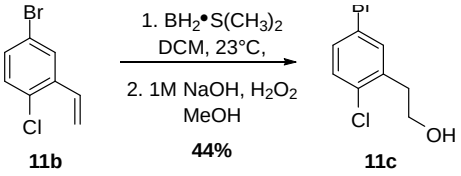

11b **11c**

Synthesis of 11c. **11b** (0.5 g, 2.30 mmol, 1 eq) was added to a flame dried 100 mL round bottom flask with a stir bar and sealed under nitrogen. DCM (28 mL, 0.08 mol/L) was added to the flask and then wrapped in aluminum foil. The flask was stirred until the oil had dissolved and then the borane dimethyl sulfide complex (0.31 mL, 3.22

mmol, 1.4 eq) was added dropwise to the flask. The flask was left stirring at room temperature for 5 hours. After 5 hours, MeOH (2.34 mL, 0.98 mol/L) followed by 1M NaOH (7.66 mL, 0.3 mol/L) followed by 30% peroxide (2.35 mL, 0.98 mol/L) were added to the flask dropwise. The flask was then covered in another layer of aluminum foil and then left stirring overnight. The reaction was quenched with concentrated HCl (10 mL) and then filtered through a celite plug and washed with DCM. The collected wash was concentrated under vacuum yielding a white solid. The solid was purified using a silica gel column (15% ethyl acetate/hexanes). The collected fractions were concentrated under vacuum yielding a clear oil (238 mg, 44%). ^{1}H NMR (500 MHz, Chloroform-*d*) δ 7.42 (d, *J* = 2.4 Hz, 1H), 7.29 (dd, *J* = 8.6, 2.4 Hz, 1H), 7.21 (d, *J* = 8.5 Hz, 1H), 3.85 (t, *J* = 6.7 Hz, 2H), 2.95 (d, *J* = 6.6 Hz, 2H).

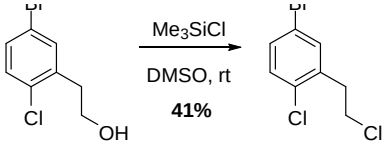

11c **11d**

Synthesis of 11d. **11c (**108 mg, 0.459 mmol, 1 eq) was added to a flame dried 25 mL round bottom flask and dried under vacuum for a few minutes before being sealed under nitrogen. Trimethylsilyl chloride (0.116 mL, 0.917 mmol, 2 eq) followed by dimethyl sulfoxide (8.5 μL, 0.119 mmol, 0.26 eq) were added to the flask. The solution was stirred for 20 minutes causing a white precipitate to crash out of solution. The solid was dissolved in methanol and concentrated under vacuum yielding a clear oil (48.4 mg, 41%). ^{1}H NMR (500 MHz, Chloroform-*d*) δ 7.42 (d, *J* = 2.2 Hz, 1H), 7.27 (dd, *J* = 8.4, 2.2 Hz, 1H), 7.20 (d, *J* = 8.4 Hz, 1H), 3.83 (t, *J* = 6.6 Hz, 2H), 2.94 (t, *J* = 6.5 Hz, 2H).

Chapter V. Supplemental Figures

V.I Cyclic Voltammetry:

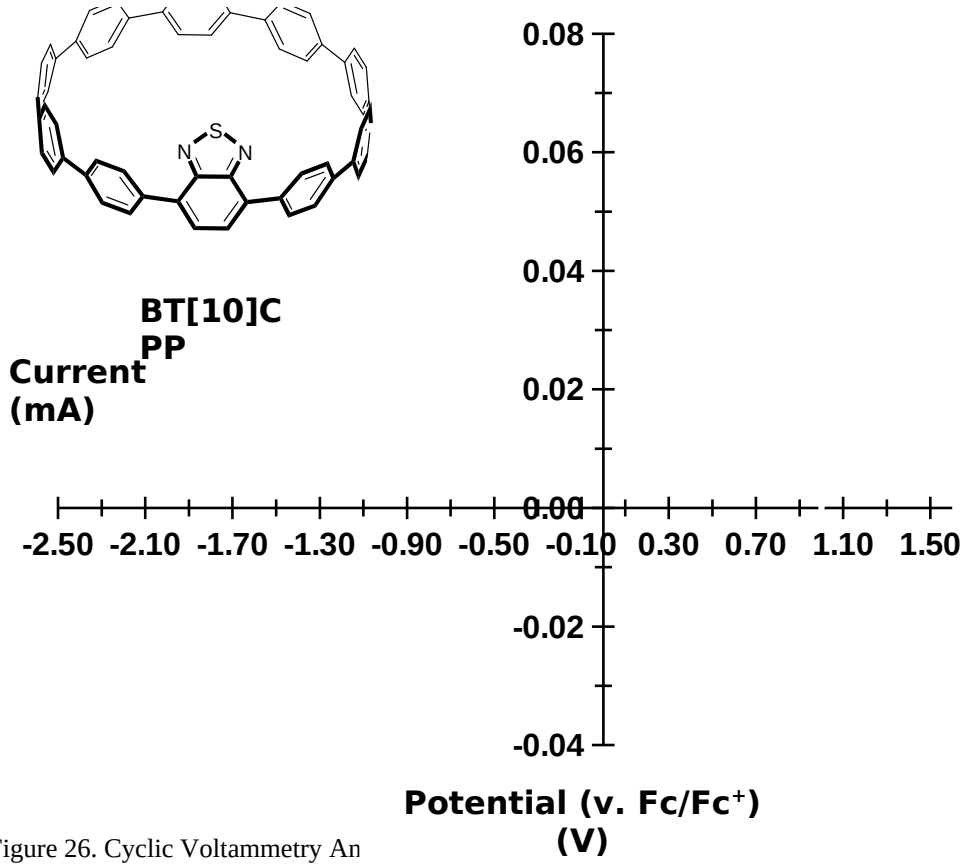

Figure 26. Cyclic Voltammetry An

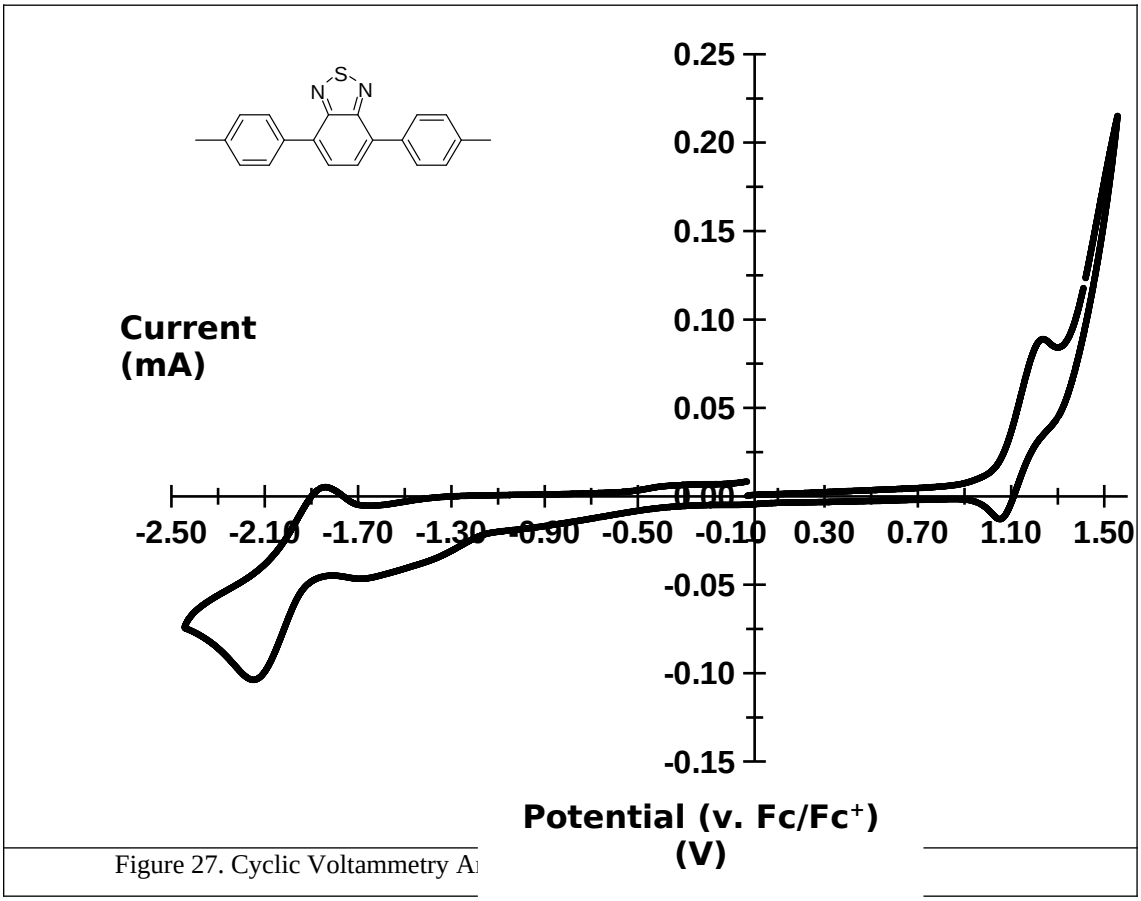

Figure 27. Cyclic Voltammetry A

5

V.II C60 Binding Constant:

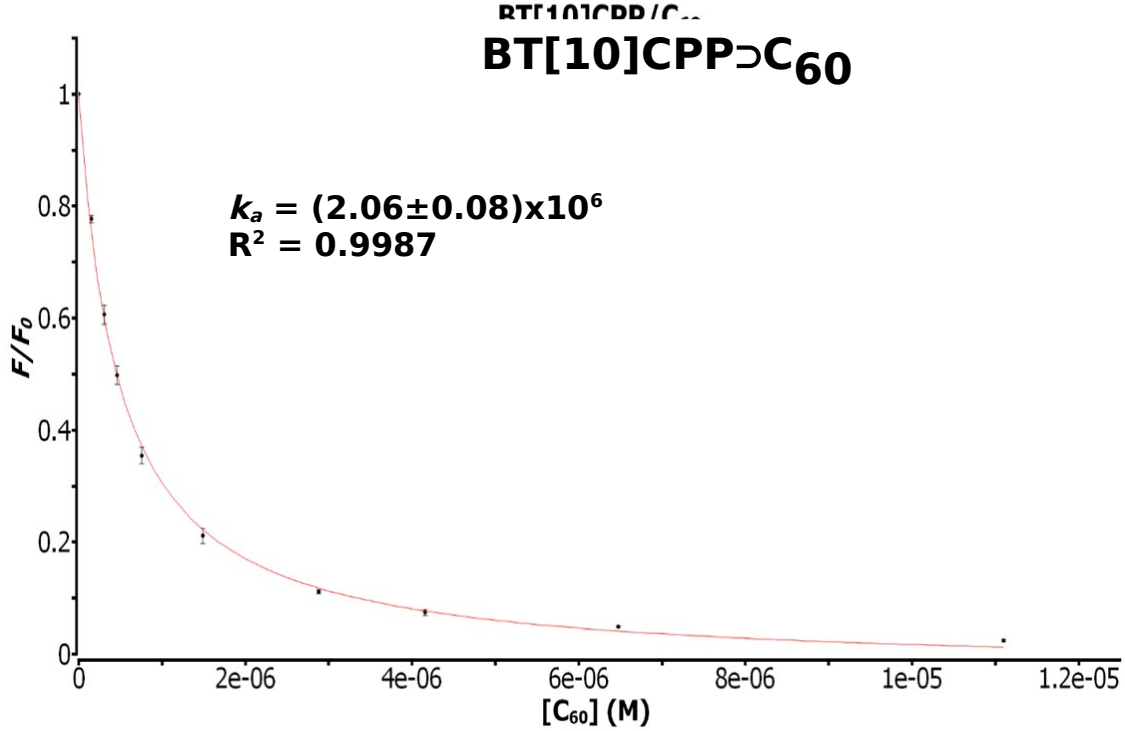

Figure 28. Binding curve of C_{60} in **BT[10]CPP**

Bibliography

(1) Fluorescence Fundamentals | Thermo Fisher Scientific - US https://www.thermofisher.com/us/en/home/references/molecular-probes-the-handbook/introduction-to-fluorescence-techniques.html (accessed May 11, 2020).

(2) Grimm, J. B.; English, B. P.; Chen, J.; Slaughter, J. P.; Zhang, Z.; Revyakin, A.; Patel, R.; Macklin, J. J.; Normanno, D.; Singer, R. H.; Lionnet, T.; Lavis, L. D. A General Method to Improve Fluorophores for Live-Cell and Single-Molecule Microscopy. *Nat. Methods* **2015**, *12* (3), 244–250.

(3) Lavis, L. D.; Raines, R. T. Bright Ideas for Chemical Biology. *ACS Chemical Biology*. American Chemical Society March 20, 2008, pp 142–155.

(4) Boyd, V.; Cholewa, O. M.; Papas, K. K. Limitations in the Use of Fluorescein Diacetate/Propidium Iodide (FDA/PI) and Cell Permeable Nucleic Acid Stains for Viability Measurements of Isolated Islets of Langerhans. *Curr. Trends Biotechnol. Pharm.* **2008**, *2* (2), 66–84.

(5) Valdes-Aguilera, O.; Cincotta, L.; Foley, J.; Kochevar, I. E. PHOTOBLEACHING OF A CYANINE DYE IN SOLUTION AND IN MEMBRANES. *Photochem. Photobiol.* **1987**, *45* (3), 337–344.

(6) Kim, K. H.; Singha, S.; Jun, Y. W.; Reo, Y. J.; Kim, H. R.; Ryu, H. G.; Bhunia, S.; Ahn, K. H. Far-Red/near-Infrared Emitting, Two-Photon Absorbing, and Bio-Stable Amino-Si-Pyronin Dyes. *Chem. Sci.* **2019**, *10* (39), 9028–9037.

(7) Lefebvre, J.; Ding, J.; Li, Z.; Finnie, P.; Lopinski, G.; Malenfant, P. R. L. High-Purity Semiconducting Single-Walled Carbon Nanotubes: A Key Enabling Material in Emerging Electronics. *Acc. Chem. Res.* **2017**, *50* (10), 2479–2486.

(8) Jasti, R.; Bhattacharjee, J.; Neaton, J. B.; Bertozzi, C. R. Synthesis, Characterization, and Theory of [9]-, [12]-, and [18]Cycloparaphenylene: Carbon Nanohoop Structures. *Journal of the American Chemical Society*. American Chemical Society December 31, 2008, pp 17646–17647.

(9) Leonhardt, E. J.; Van Raden, J. M.; Miller, D.; Zakharov, L. N.; Alemán, B.; Jasti, R. A Bottom-Up Approach to Solution-Processed, Atomically Precise Graphitic Cylinders on Graphite. *Nano Lett.* **2018**, *18* (12), 7991–7997.

(10) Maust, R.; Li, P.; Zakharov, L. N.; Jasti, R. Cycloparaphenylene-Norbornene Monomers Afford Access to Carbon Nanohoop-Based Polymers. *ChemRxiv* **2019**, 1–28..

(11) Van Raden, J. M.; Darzi, E. R.; Zakharov, L. N.; Jasti, R. Synthesis and

Characterization of a Highly Strained Donor-Acceptor Nanohoop. *Org. Biomol. Chem.* **2016**, *14* (24), 5721–5727.

(12) Patel, V. K.; Kayahara, E.; Yamago, S. Practical Synthesis of [*n*]Cycloparaphenylenes (*n* =5, 7-12) by H_2SnCl_4-Mediated Aromatization of 1,4-Dihydroxycyclo-2,5-Diene Precursors. *Chem. - A Eur. J.* **2015**, *21* (15), 5742–5749.

(13) Lovell, T. C.; Colwell, C. E.; Zakharov, L. N.; Jasti, R. Symmetry Breaking and the Turn-on Fluorescence of Small, Highly Strained Carbon Nanohoops. *Chem. Sci.* **2019**, *10* (13), 3786–3790.

(14) Darzi, E. R.; Jasti, R. The Dynamic, Size-Dependent Properties of [5]-[12]Cycloparaphenylenes. *Chemical Society Reviews*. Royal Society of Chemistry September 21, 2015, pp 6401–6410.

(15) Urano, Y.; Kamiya, M.; Kanda, K.; Ueno, T.; Hirose, K.; Nagano, T. Evolution of Fluorescein as a Platform for Finely Tunable Fluorescence Probes. *J. Am. Chem. Soc.* **2005**, *127* (13), 4888–4894.

(16) White, B. M.; Zhao, Y.; Kawashima, T. E.; Branchaud, B. P.; Pluth, M. D.; Jasti, R. Expanding the Chemical Space of Biocompatible Fluorophores: Nanohoops in Cells. *ACS Cent. Sci.* **2018**, *4* (9), 1173–1178.

(17) Kuwabara, T.; Orii, J.; Segawa, Y.; Itami, K. Curved Oligophenylenes as Donors in Shape-Persistent Donor-Acceptor Macrocycles with Solvatofluorochromic Properties. *Angew. Chemie Int. Ed.* **2015**, *54* (33), 9646–9649.

(18) Sonar, P.; Williams, E. L.; Singh, S. P.; Dodabalapur, A. Thiophene-Benzothiadiazole-Thiophene (D-A-D) Based Polymers: Effect of Donor/Acceptor Moieties Adjacent to D-A-D Segment on Photophysical and Photovoltaic Properties. *J. Mater. Chem.* **2011**, *21* (28), 10532–10541.

(19) Davies, D. L.; Lowe, M. P.; Ryder, K. S.; Singh, K.; Singh, S. Tuning Emission Wavelength and Redox Properties through Position of the Substituent in Iridium(Iii) Cyclometallated Complexes. *Dalt. Trans.* **2011**, *40* (5), 1028–1030.

(20) Iwamoto, T.; Watanabe, Y.; Sadahiro, T.; Haino, T.; Yamago, S. Size-Selective Encapsulation of C60 by [10]Cycloparaphenylene: Formation of the Shortest Fullerene-Peapod. *Angew. Chemie Int. Ed.* **2011**, *50* (36), 8342–8344.

(21) Panchuk-Voloshina, N.; Haugland, R. P.; Bishop-Stewart, J.; Bhalgat, M. K.; Millard, P. J.; Mao, F.; Leung, W. Y.; Haugland, R. P. Alexa Dyes, a Series of New Fluorescent Dyes That Yield Exceptionally Bright, Photostable Conjugates. *J. Histochem. Cytochem.* **1999**, *47* (9), 1179–1188.

(22) Golder, M. R.; Colwell, C. E.; Wong, B. M.; Zakharov, L. N.; Zhen, J.; Jasti, R. Iterative Reductive Aromatization/Ring-Closing Metathesis Strategy toward the Synthesis of Strained Aromatic Belts. *J. Am. Chem. Soc.* **2016**, *138* (20), 6577–6582.